# Global and National $CO_2$ Emission from Lime Production Process and Carbonation sink from 1930 to 2024

Longfei Bing[1,3,4#], Xiaoyu Zhang[1,5#], Le Niu[1,5,7], Zhi Cao[7], Jiaoyue Wang[1,3,4*], Jiajie Li[2], Xue Jiang[2,6], Fengming, Xi[1,2,3,4*]

1 Key Laboratory of Forest Ecology and Silviculture, Institute of Applied Ecology, Chinese Academy of Sciences, Shenyang 11001, China

2 Institute of Mineral Resources, University of Science and Technology Beijing, Beijing, 100083, China

3 Key Laboratory of Terrestrial Ecosystem Carbon Neutrality, Shenyang 110016, China

4 National-Local Joint Engineering Laboratory of Contaminated Soil Remediation by Bio-physicochemical Synergistic Process, Shenyang 110016, China

5 University of Chinese Academy of Sciences, Beijing 100049, China

6 Baowu Resources Co., Ltd., Shanghai 201206, China

7 Institute of Surface-Earth System Science, School of Earth System Science, Tianjin University, Tianjin 300072, China.

# These authors contributed equally to this work.

*Correspondence to: Fengming Xi (xifengming@ustb.edu.cn); Jiaoyue Wang (wangjiaoyue@iae.ac.cn )

**Abstract**

Accurate quantification of lime process emissions and subsequent carbonation uptake is needed to represent the lime carbon cycle in global carbon-budget assessments. We developed a source-prioritized and internally cross-checked dataset for 1930–2024 by harmonizing USGS statistics, national statistical yearbooks, industrial records, and explicitly identified proxy-based reconstructions. The framework resolves 11 major lime-producing countries, collectively representing 78.9% of global lime production, and derives country-specific process-emission factors from sectoral lime-use structures and CaO-content requirements. Annual global lime carbonation uptake increased from 4.1 Mt $CO_2$ $yr^{-1}$ (95% CI: 3.5–4.8 Mt $CO_2$ $yr^{-1}$) in 1930 to 136.1 Mt $CO_2$ $yr^{-1}$ (95% CI: 107.9–171.5 Mt $CO_2$ $yr^{-1}$) in 2024, corresponding to a compound annual growth rate of 3.8%. Cumulative process emissions reached 11.3 Gt $CO_2$ (95% confidence interval (CI): 10.7–11.9 Gt $CO_2$), of which construction and metallurgy contributed 3.9 Gt $CO_2$ (34.5%) and 3.8 Gt $CO_2$ (33.5%), respectively. Cumulative carbonation uptake reached 4.8 Gt $CO_2$ (95% CI: 3.9–5.8 Gt $CO_2$), offsetting 42.2% of process emissions, 3.4% higher than the 38.8% estimate for 1930–2020 reported by Bing et al. (2023). China contributed 5.5 Gt $CO_2$ of process emissions (48.3% of the global total) and 1.9 Gt $CO_2$ of carbonation uptake (40.7%). Uncertainties associated with data sources, historical reconstruction, and material parameters were propagated through 10,000 Monte Carlo iterations. Metallurgical by-products and construction materials dominated cumulative uptake. Country-level trajectories

indicate that most developed economies have passed their lime process-emission peaks, whereas China remains on a growth trajectory and Brazil retains substantially higher emissions than its early historical levels despite a modest decline after its 2013 peak. This dataset provides a consistent empirical basis for representing lime-related carbon sources and sinks in global carbon-cycle assessments and is archived on Zenodo at https://doi.org/10.57760/sciencedb.45314 (Bing et al., 2026).

Abbreviations and symbols

| Abbreviation / symbol | Definition |
|---|---|
| BFS | Blast furnace slag |
| CEF | Carbon emission factor |
| CI | Confidence interval |
| CS | Carbide slag |
| GCB | Global Carbon Budget |
| IPCC | Intergovernmental Panel on Climate Change |
| IPPU | Industrial Processes and Product Use |
| LKD | Lime kiln dust |
| LM | Paper-mill lime mud |
| LSS | Lime-stabilized soil |
| MFA | Material Flow Analysis |
| MOR | Lime mortar |
| PCC | Precipitated calcium carbonate |
| RM | Red mud |
| ROW | Rest of the world |
| SS | Steel slag |
| SUG | Carbonation sugar |
| USGS | United States Geological Survey |

## 1. Introduction

Lime serves as an indispensable feedstock in numerous industrial processes, playing a pivotal role in sectors such as steelmaking, construction materials, chemical engineering, and wastewater treatment (Revuelta, 2021). Over the past two decades, driven by urbanization, industrialization, and the accelerated development of large-scale infrastructure, global lime production has surged by 0.68-fold, rising from 250 Mt in 2004 to 420 Mt in 2024 (USGS, 2026a). Projections indicate that two-thirds of the global population will reside in urban areas by 2050 (UN-Habitat, 2022). This continuous urbanization process is expected to further drive the demand for housing, transportation, infrastructure, and environmental sanitation facilities, thereby leading to sustained increase in the consumption of lime as a fundamental material.

Lime production is carbon intensive because $CO_2$ is released by carbonate calcination, with additional emissions from kiln fuels and electricity. Calcination generally accounts for

about two-thirds of total lime-production-related $CO_2$ emissions, while energy use contributes much of the remainder (Han et al., 2022; Laveglia et al., 2024a). Following IPCC inventory boundaries, this study quantifies process emissions from lime production and the subsequent carbonation uptake of lime-derived materials; energy-related emissions are excluded to avoid overlap with the energy sector. Because process emissions are governed by carbonate decomposition, they cannot be eliminated solely through fuel switching or energy-efficiency improvements, making lime a hard-to-abate industrial sector (Davis et al., 2018).

Existing carbon emission inventories and global carbon budget assessments treat lime production and subsequent carbonation uptake inconsistently. CDIAC-FF provides long-term global and national $CO_2$ emission series for fossil fuel combustion, gas flaring, and cement manufacture, but does not include process emissions from lime production (Gilfillan and Marland, 2021). MEIC-global-$CO_2$ improves source-category resolution and incorporates subnational information for major emitters, but mainly focuses on fossil-fuel combustion and cement-related $CO_2$ emissions and does not provide a dedicated, globally consistent representation of lime-production emissions and lime-product carbonation uptake (Xu et al., 2024). EDGAR provides a comprehensive national and gridded greenhouse gas emission inventory covering multiple sectors and industrial processes, however, its framework is emissions-oriented and does not quantify $CO_2$ uptake resulting from the carbonation of lime products during their use and disposal stages (Crippa et al., 2024). The Global Carbon Budget has incorporated cement carbonation uptake as a negative flux within the fossil $CO_2$ component, but explicitly notes that lime-production emissions are not yet globally covered. Current estimates include lime-production emissions for China and the United States, whereas most non-Annex I countries and emissions from other Annex I countries before 1990 remain unaccounted (Friedlingstein et al., 2025). Consequently, existing datasets generally cover only part of the lime carbon cycle: some omit lime process emissions, some focus primarily on carbonate decomposition associated with cement manufacture, and others include lime process emissions but do not couple them with the subsequent carbonation sink of lime products. To our knowledge, a standardized, country-resolved, long-term dataset with a consistent system boundary that jointly quantifies lime process emissions and carbonation sink is still lacking, limiting the comprehensive integration of lime-related carbon budget and sinks into both global carbon cycle science and Global Carbon Budget.

However, accurately quantifying process emissions from the global lime industry remains a significant challenge, primarily due to data gaps and inconsistent statistical frameworks. First, large volumes of lime are produced for internal use by steel, sugar, and chemical enterprises, which does not enter commercial circulation. The prevalence of this "captive production" leads to omit much of the output and severely underestimate the official activity data (USGS, 2026a). Second, significant disparities in kiln technology exist across regions. The coexistence of traditional vertical kilns in developing countries and high-efficiency rotary kilns in developed countries leads to substantial fluctuations in emission factors (European Commission, 2013). As has been noted, accurate estimation of emission factors depends heavily on the precise characterization of raw-material composition (Andrew, 2019). Ignoring these variations results in significant process emissions estimation biases. Furthermore, overlapping statistical boundaries between lime and cement production often lead to misclassification or omissions in

historical data, which making it is difficult for existing databases to reflect the true emission trajectory of lime industry (Andrew, 2019). According to the China Building Materials Federation, total $CO_2$ emissions from China's building materials industry reached 1.48 billion tons in 2020, representing 14.9% of the national total, with the lime sector contributing approximately 8.1% of the industry's emissions (CBMEMA, 2026). Globally, the lime industry contributes approximately 1% of total anthropogenic $CO_2$ emissions (Campo et al., 2021; Friedlingstein et al., 2022). Notably, lime is extensively utilized in iron and steel, construction, chemical engineering, agriculture, and environmental remediation (European Commission, 2013). During their lifecycle, the produced lime-based materials undergo carbonation with atmospheric $CO_2$ via Eqs. (1) and (2), thereby sequestering a portion of the process $CO_2$ released by their production (Simoni et al., 2022). Previous studies revealed that between 1930 and 2020, global lime materials cumulatively sequestered approximately 529.7 Mt $CO_2$ (95% CI: 372.6–719.0 Mt $CO_2$), offsetting 38.83% of process emissions over the same period (Bing et al., 2023).

$$CaO + H_2O = Ca(OH)_2 \quad \text{Eq (1)}$$

$$Ca(OH)_2 + CO_2 = CaCO_3 + H_2O \quad \text{Eq (2)}$$

Carbonation represents a pivotal pathway for achieving net-zero emissions in the lime industry. Although previous studies have indicated that $CO_2$ emissions from lime production can be mitigated by substituting fossil fuels with residue-derived fuels (Zementwerke eV, 2021), replacing calcium carbonate calcination with electrochemical (Ellis et al., 2020), and chemical decarbonization methods (Hanein et al., 2021), these approaches are currently constrained by high costs and technical complexities and making challenges in large-scale deployment (Simoni et al., 2022). Consequently, carbon sequestration via carbonation plays an alternative role in the decarbonization of the lime sector, which creating an urgent need to accurately quantify its contribution. Currently, China's Action Plan for Carbon Peaking by 2030 in the Building Materials Industry promotes utilization of industrial solid wastes, such as steel slag and carbide slag (MIIT, 2026). Similarly, the European Lime Association explicitly identifies Carbon Capture, Utilization, and Storage (CCUS) and natural carbonation as critical measures, aiming to achieve $CO_2$ negative emissions by 2050 through technological upgrades (EuLA, 2026a). The National Lime Association (NLA, 2023) in the United States also released a roadmap targeting carbon neutrality by 2050, emphasizing the significance of the carbon sink function of lime products. At present, the Global Carbon Budget (GCB) has incorporated cement carbonation sink into the anthropogenic $CO_2$ sink (Friedlingstein et al., 2022). However, the lime carbonation sink remains excluded. For context, carbon uptake by cement materials in 2021 accounted for approximately 8.23% of the global mean land carbon sink from 2010–2020 (Huang et al., 2023; Friedlingstein et al., 2020), whereas lime materials sequestered an amount equivalent to approximately 1.09% of the mean land sink from 2012–2020 (Bing et al., 2023). Incorporating the lime carbonation sink into the GCB would provide a more accurate reflection of the global carbon cycle and optimize regional carbon budget allocations. Therefore, an accurate accounting of lime carbonation sink is indispensable.

Previous efforts by our team provided a preliminary accounting of lime-based carbonation sink in China and the United States (Bing et al., 2023). However, the study treated the rest of the world as a homogeneous entity. It overlooks the significant divergence in process carbon emissions and sequestration coefficients caused by variations in production technologies, raw

material compositions, and application industries across different nations. In particular, the carbon sequestration of metallurgical wastes has been historically underestimated. For instance, pig iron production requires the addition of quicklime and limestone as metallurgical fluxes (Yang et al., 2024). The resulting slag, with calcium oxide (CaO) content ranging from 30% to 50% (Ren et al., 2021), presents substantial carbon sequestration (Elyasi Gomari et al., 2024), which is also one of key improvements of this study. Furthermore, global production rates of iron and steel slag have generally declined due to optimized furnace lining materials and refined blowing processes (Naito et al., 2015). Concurrently, the resource utilization of these materials has continued to improve. On a global scale, blast furnace slag (BFS) and steel slag (SS) are widely repurposed for cement production, road construction, building materials, and fertilizers (Heraiz et al., 2025). However, significant disparities exist at the national level. The developed nations have achieved comprehensive utilization rates of steel slag exceeding 90%, while the rate in China remains approximately 20% (Gao et al., 2023). By accounting for these technological and regional discrepancies, this study provides a more robust quantification of the global lime process emissions and carbonation sink.

To improve the accuracy and transparency of global lime-carbon accounting, this study makes four principal advances. (1) Source-prioritized activity-data reconstruction: USGS statistics, national yearbooks, and industry records were harmonized for 11 major producing countries, representing 78.9% of global output, with proxy-derived and interpolated values explicitly identified (Supplementary Table SI-2, Data 1). (2) Composition-sensitive process-emission factors: following Liu et al. (2015), sector-specific CaO requirements and national lime-use structures were combined to derive country-level weighted emission factors (Supplementary Table SI-3, Data 1). (3) A consistent material-flow boundary: lime-derived CaO was traced across production, construction, metallurgical, and chemical pathways while excluding non-lime CaO inputs. (4) Data-constrained temporal and regional parameterization: SS and BFS generation and pathway-allocation parameters were assigned for 1930–1949, 1950–1972, 1973–1999, and 2000–2024, using country-specific data where available and documented regional assumptions otherwise. These intervals are common accounting windows and do not imply synchronized technological transitions among countries.

## 2. Methodology and Data Sources

### 2.1. Estimation of Process $CO_2$ Emissions from Lime Production

Calculations were conducted using the Tier 2 method from the 2006 IPCC Guidelines for National Greenhouse Gas Inventories (IPCC, 2006), considering $CO_2$ emissions generated solely from limestone calcination. The calculation formula is as follows:

$$E_{process,i} = P_{lime,i} \times EF_{lime,i} \quad (3)$$

where, $E_{process,i}$ represents the industrial process $CO_2$ emissions from the lime industry in country $i$; $P_{lime,i}$ denotes the annual lime production of country $i$; $EF_{lime,i}$ is the $CO_2$ emission factor for lime production in country $i$.

Carbon emission factors (CEFs) were calculated following the Tier 2 approach for lime production in the 2006 IPCC Guidelines for National Greenhouse Gas Inventories (IPCC, 2006). Under this approach, process $CO_2$ emissions are derived from the stoichiometric relationship between $CO_2$ and carbonate-derived CaO or CaO·MgO in lime products. In this study, sector-specific CaO contents were compiled for lime used in major end-use sectors, including

metallurgy, construction, and the chemical industry. Because lime quality and CaO content differ among end-use sectors, these sectoral categories were used as practical proxies for product composition. Sector-specific emission factors were first derived by multiplying the CaO or CaO·MgO content of lime used in each sector by the corresponding IPCC stoichiometric ratio. Country-specific average CEFs were then calculated as weighted averages of sector-specific emission factors according to the lime-use shares of each sector. This approach is consistent with the IPCC Tier 2 principle of deriving emission factors from lime composition, while allowing national differences in lime-use structure and product quality to be reflected. Detailed CaO contents, sectoral lime-use shares, assumptions, and literature sources are provided in Supplementary Table SI-3 Data 1.

### 2.2. Estimation of $CO_2$ Uptake by Lime

The system boundary was established using material flow analysis (MFA; Fig. 1), based on the lime-carbonation framework of Liu et al. (2018). It includes ten lime-based materials classified by lifecycle stage. Lime kiln dust (LKD) is treated as a direct by-product of lime production. The remaining nine materials are grouped into three downstream sectors: metallurgy, including steel slag (SS), blast furnace slag (BFS), and red mud (RM); chemicals, including precipitated calcium carbonate (PCC), carbide slag (CS), carbonation sugar (SUG), and paper mill lime mud (LM); and construction, including lime-stabilized soil (LSS) and lime mortar (MOR). Most material flows follow Liu et al. (2018), while BFS is newly included to improve the accounting boundary.

To avoid double counting with existing cement-carbonation datasets, the system boundary for metallurgical slags (SS and BFS) is defined by the origin of CaO rather than by the subsequent use of the slag. Only CaO derived from lime fluxes and represented in the lime production activity data is attributed to the lime carbonation sink. CaO originating from iron ore, gangue minerals, limestone, dolomite, or other non-lime inputs is excluded. Although some SS and BFS are later used in cement or clinker production, existing cement-carbonation inventories do not account for the carbonation of lime-derived CaO in metallurgical slags, particularly BFS. Therefore, including this lime-derived CaO does not overlap with existing cement-carbonation estimates.

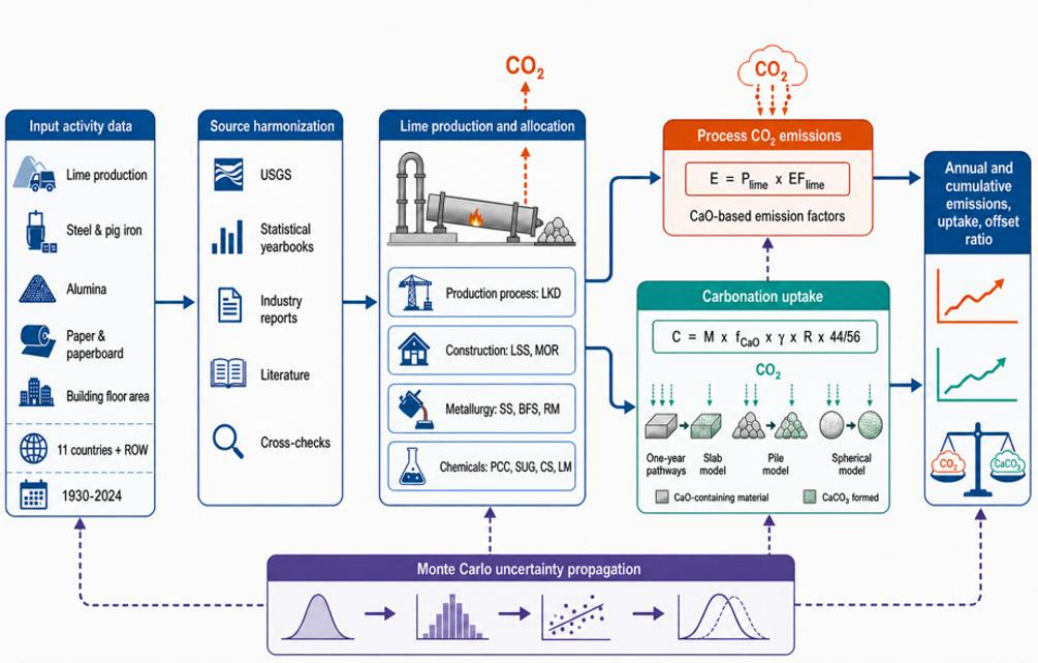


Fig. 1. Methodological framework for lime process-emission and carbonation-uptake accounting.

### 2.2.1. General Calculation Model

**(1) Carbon Sequestration**

For each lime-derived material pathway, $CO_2$ uptake is calculated from material mass, CaO content, and the pathway-specific effective CaO conversion fraction:

$$C_m = M_m \times f_{CaO,m} \times \Phi_m \times \frac{M_{CO2}}{M_{CaO}} \quad (4)$$

where $M_m$ is the mass of material $m$, $f_{CaO,m}$ is its CaO mass fraction, and $\Phi_m$ is the effective fraction of CaO converted to $CaCO_3$ within the corresponding pathway. The pathway-specific treatment of $\Phi_m$ is defined as follows:

$$\Phi_m = 1 \quad (\mathrm{PCC, SUG}) \quad (5)$$

$$\Phi_m = \gamma_m \times R_m(\mathrm{a}) \quad (\mathrm{LSS, MOR, SS, BFS}) \quad (6)$$

$$\Phi_m = \bar{\gamma}_{m,1} \quad (\mathrm{LKD, LM, RM, CS}) \quad (7)$$

For PCC and SUG, carbonation is integral to production and $\Phi_m$ is set to 1 (Wang and Shen, 2002). For LSS, MOR, SS, and BFS, $\gamma_m$ is the material-specific ultimate CaO conversion fraction and $R_m(a)$ is the cumulative fraction of that ultimate extent reached at material age $a$. Thus, $\gamma_m \times R_m(a)$ represents the cumulative proportion of CaO converted by that age. $R_m(a) = 1$ indicates that the pathway-specific ultimate extent has been reached, but does not imply conversion of all CaO unless $\gamma_m = 1$. For LKD, LM, RM, and CS, the evaluation age is fixed at one year and $\Phi_m$ is represented by $\bar{\gamma}_{m,1}$, the literature-reported pile-average CaO conversion fraction reached after one year. The reported average values and ranges are used directly in the Monte Carlo analysis. The stoichiometric molar-mass ratio $M_{CO_2}/M_{CaO}$ is 44/56.

The conversion factor $\gamma$ and temporal function $R$ therefore describe different processes.

The former constrains the ultimate chemically available CaO fraction, whereas the latter represents progression toward that extent. Model selection follows the order shown in Fig. 2. LSS and MOR use the slab model (Fig. 2a). The layered stockpile representation for LKD, LM, RM, and CS (Fig. 2b) explains rapid carbonation near the exposed surface and lower conversion at greater depths because of restricted $CO_2$ transport and successive covering by newly deposited material. SS and BFS use the spherical-particle model (Fig. 2c). Material-specific conversion and uncertainty parameters are provided in Supplementary Table SI-3, Data 10 and Data 14.

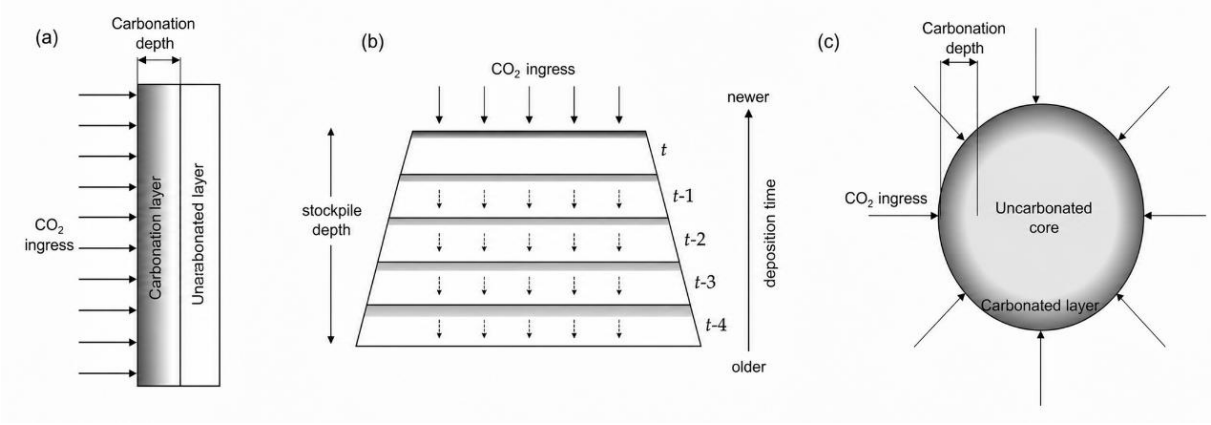


Fig. 2. Schematic carbonation representations: (a) slab model for LSS and MOR; (b) layered stockpile mechanism for LKD, LM, RM, and CS; and (c) spherical-particle model for SS and BFS.

Complete annual, country-specific CaO-content data were not available for all countries. We therefore compiled reported CaO contents from peer-reviewed studies, technical standards, and reports issued by national authorities and industry associations. For lime products, the compilation considered differences among high-calcium, dolomitic, and hydraulic lime, as well as variations in product purity among construction, metallurgical, and chemical applications. CaO-content data for SS, BFS, RM, and LM were compiled using the same procedure. Depending on the available data, triangular distributions defined by minimum, central, and maximum values or normal distributions defined by means and standard deviations were constructed for the Monte Carlo analysis. All CaO-content observations, material classifications, references, and distribution parameters are provided in Supplementary Table SI-3, Data 7.

Because production data disaggregated by high-calcium, dolomitic, and hydraulic lime were unavailable for many countries and historical periods, this approach should not be interpreted as a complete IPCC Tier 2 implementation. Instead, it represents a literature-based probabilistic parameterization of compositional uncertainty.

**(2) Annual Carbonation Ratio**

Quantitative time-dependent carbonation functions were applied to the slab and spherical-particle pathways. For these geometries, carbonation depth follows the square-root-of-time relationship:

$$d = k \times \sqrt{t} \quad (8)$$

where k is a material-specific carbonation-rate coefficient and t is material age (Papadakis

et al., 1991; Johannesson and Utgenannt, 2001). The carbonation depth is converted to a carbonated fraction according to material geometry.

For the slab model, the annual carbonation ratio is calculated as:

$$R_{lime} = \left(d_{lime,i} - d_{lime,i-1}\right)/d_T \quad (9)$$

where $d_{lime,i}$ and $d_{lime,i-1}$ are the carbonation depths at the end of years $i$ and $i-1$, respectively, and $d_T$ is the design thickness of the lime-based material. The resulting $R$ value is expressed as a decimal fraction in the calculations.

For fine-particle stockpiles, the carbonation age is fixed at one year. Because the CaO conversion fraction generally decreases with stockpile depth, the one-year pile-average conversion fraction is expressed as:

$$\bar{\gamma}_{m,1} = \frac{1}{H_m}\int_0^{H_m} \gamma_m(z,1)dz \quad (10)$$

where $H_m$ is the stockpile height and $\gamma_m(z,1)$ is the CaO-to-$CaCO_3$ conversion fraction of material $m$ at depth $z$ after one year. Thus, $\bar{\gamma}_{m,1}$ represents the mean conversion fraction over the full stockpile depth. Because continuous depth profiles were unavailable for all materials and countries, the calculation directly adopts the literature-reported one-year pile-average value and its range in the Monte Carlo analysis, without introducing additional depth-profile parameters. The observed decrease in conversion with stockpile depth provides the physical basis for this treatment (Muriithi et al., 2013).

For the spherical-particle model, the annual carbon-uptake ratio is calculated as:

$$R_{lime,i} = \begin{cases} 100\% - \dfrac{\int_a^b \frac{\pi}{6}(D-D_{slag})^3}{\int_a^b \frac{\pi}{6}D^3} \times 100\% & (a > D_{slag}) \\ 100\% - \dfrac{\int_{D_0}^b \frac{\pi}{6}(D-D_{slag})^3}{\int_a^b \frac{\pi}{6}D^3} \times 100\% & (a \le D_{slag} \le b) \\ 100\% & (b < D_{slag}) \end{cases} \quad (11)$$

where $D$ is slag-particle diameter; $D_{slag}$ is the maximum diameter of the completely carbonated portion of an SS or BFS particle; $a$ and $b$ are the minimum and maximum particle diameters in the adopted particle-size distribution; and $D_{slag} = 2d_{slag,i} = 2k_{slag}\sqrt{t_i}$. Here, $d_{slag,i}$ is carbonation depth at age $t_i$ and $k_{slag}$ is the slag-specific carbonation-rate coefficient. Percentage values from Eq. (11) are converted to decimal fractions before being used in Eq. (4).

**(3) Calculation of Annual and Cumulative Carbon Uptake**

For the time-dependent pathways LSS, MOR, SS, and BFS, cumulative uptake is evaluated by production cohort and material age. Annual uptake is then obtained as the increment between consecutive calendar years:

$$C_{m,t}^{ann} = C_{m,t}^{cum} - C_{m,t-1}^{cum} \quad (12)$$

where $C_{m,tann}$ is uptake by material m during year $t$ and $C_{m,tcum}$ is cumulative uptake through year $t$. For PCC and SUG, uptake is assigned to the production year because carbonation is integral to production. For LKD, LM, RM, and CS, uptake is calculated at a fixed carbonation age of one year from the material mass generated or stockpiled in year $t$ and the corresponding one-year pile-average conversion fraction.

## 2.2.2. Details of Material-Specific Calculations

**(1) Lime material from the production process (LKD)**

LKD is generated during lime calcination. Its uptake attributed to year t is calculated as:

$$M_{lkd} = m_{lime} \times r_{lkd} \quad (13)$$

where $r_{lkd}$ represents the industry default generation rate of kiln dust. Due to its fine particle size and high specific surface area, LKD can undergo rapid carbonation during stockpiling, but its carbonation ratio was not assumed to be 100%; the parameter values are provided in Supplementary Table SI-3 Data14 and 17.

**(2) Lime materials in the construction industry (LSS and MOR)**

LSS production is calculated as:

$$M_{lss} = m_{lime} \times L_1 \times a_1 \quad (14)$$

where $m_{lime}$ is lime production, $L_1$ is the fraction of lime used in construction, and $a_1$ is the share of construction lime allocated to LSS. The slab-model annual carbonation ratio and carbonation depth are:

$$R_{lss} = \frac{d_{lss,i} - d_{lss,i-1}}{d_T} \quad (15)$$

$$d_{lss} = k_{lss} \times \sqrt{t_{lss}} \quad (16)$$

where $d_T$ is the design thickness of LSS, $d_{lss,i}$ is carbonation depth at the end of year $i$, $k_{lss}$ is the LSS-specific carbonation-rate coefficient, and $t_{lss}$ is carbonation age.

MOR production is calculated as:

$$M_{mor} = m_{lime} \times L_1 \times a_2 \quad (17)$$

where $a_2$ is the share of construction lime allocated to MOR. To avoid double counting with cement-carbonation datasets, MOR includes only commercial lime used in construction and excludes CaO derived from cement-clinker hydration. Its annual carbonation ratio and carbonation depth are:

$$R_{mor} = \frac{d_{mor,i} - d_{mor,i-1}}{d_T} \quad (18)$$

$$d_{mor} = k_{mor} \times \sqrt{t_{mor}} \quad (19)$$

where $d_T$ is mortar design thickness, $d_{mor,i}$ is carbonation depth at the end of year $i$, $k_{mor}$ is the MOR-specific carbonation-rate coefficient, and $t_{mor}$ is carbonation age.

**(3) Lime materials in the metallurgical industry (SS, BFS, and RM)**

Total SS production is estimated from crude-steel output as:

$$M_{ss,total} = m_{crude\ steel} \times r_{ss} \quad (20)$$

where rss is the time-dependent SS generation rate reported in Supplementary Table SI-3, Data 1. The SS mass included in natural-carbonation accounting is:

$$M_{ss} = M_{ss,total} \times U_{ss} \quad (21)$$

where Uss is the combined fraction of SS used in road-base applications or stored in open-air stockpiles. It is a pathway-allocation parameter and does not affect estimated total SS production. Carbonation of this fraction is calculated using the spherical-particle model in Eq. (11).

The BFS mass included in natural-carbonation accounting is:

$$M_{bfs} = m_{bfs} \times r_{bfs} \times l_{bfs} \times U_{bfs} \quad (22)$$

where $m_{bfs}$ represents blast-furnace iron production; $r_{bfs}$ is the BFS generation rate, with time-dependent values provided in Supplementary Table SI-3, Data 1; $l_{bfs}$ is the proportion of CaO in BFS derived specifically from lime input; and $U_{bfs}$ is the combined fraction of total BFS directed to road-base applications or stored in open-air stockpiles and therefore included in the natural-carbonation accounting. By isolating the lime-derived CaO fraction, $l_{bfs}$ prevents boundary overlap with clinker-based cement-carbonation accounting, including when BFS is subsequently used as a supplementary cementitious material. $U_{bfs}$ is not the ratio of open-air stockpiling to road-base use and does not affect the estimated total production of BFS. It is a pathway-allocation parameter used only to identify the fraction of total BFS included within the natural-carbonation boundary. Carbonation of this fraction is calculated using the spherical-particle model described in Eq. (11).

It should be noted that $U_{ss}$ and $U_{bfs}$ represent the fractions of SS and BFS, respectively, used in road-base applications or stored in open-air stockpiles and therefore included in the natural-carbonation accounting. These parameters differ from the overall utilization rates described earlier, which represent the proportions of slag recycled through all resource-utilization pathways. SS and BFS used in road-base applications or stored in open-air stockpiles can react with atmospheric or pore-water $CO_2$. However, the actual extent of carbonation depends strongly on slag mineralogy, particle size, gas and moisture transport conditions, and other factors (Pullin et al., 2019; Chukwuma et al., 2021; Elyasi Elyasi Gomari et al., 2024). Slag incorporated into other valorized products is considered to enter downstream product systems. Because its subsequent carbonation depends on product-specific service and exposure conditions, it is excluded from the present accounting (Li et al., 2022). Therefore, exclusion of this fraction from the equations indicates only that its carbonation lies outside the accounting boundary of this study, rather than that its actual carbonation is zero.

The lime-derived CaO fraction in BFS was determined using an ironmaking-burden mass-balance approach. First, quicklime consumption per tonne of pig iron was estimated from the total blast-furnace burden consumption per tonne of pig iron, the shares of sinter, pellets, and lump ore in the burden, and quicklime consumption per tonne of sinter. The resulting quicklime input was converted to lime-derived CaO and divided by the total CaO contained in the generated BFS, which was calculated from the BFS generation rate and BFS CaO content. Country- and period-specific parameters used in this calculation are provided in Supplementary Table SI-3, Data 15.

For RM, uptake attributed to the annual stockpiled material flow is calculated as:

$$C_{RM,t} = M_{alumina,t} \times r_{RM,t} \times (1 - U_{RM,t}) \times f_{CaO,RM} \times \bar{\gamma}_{RM,1} \times \frac{M_{CO2}}{M_{CaO}} \quad (23)$$

where $M_{alumina,t}$ is alumina production, $r_{RM,t}$ is the RM generation rate, $U_{RM,t}$ is the recycling and utilization rate, and $\bar{\gamma}_{RM,1}$ is the one-year pile-average CaO conversion fraction. The residual fraction is treated as stockpiled material. The literature-reported average conversion and range are used in the Monte Carlo analysis.

**(4) Lime materials in the chemical industry (PCC, SUG, CS, and LM)**

PCC and SUG production is calculated as:

$$M_{pcc} = m_{lime} \times L_2 \times b \quad (24)$$

where $L_2$ is the fraction of total lime used in the chemical sector and $b$ is the share allocated

to PCC or SUG production. Because carbonation is integral to these production pathways, $\Phi m$ is set to 1 in Eq. (4).

For LM, uptake attributed to the annual stockpiled material flow is calculated as:

$$C_{LM,t} = M_{paper,t} \times r_{LM,t} \times (1 - U_{LM,t}) \times f_{CaO,LM} \times \bar{\gamma}_{LM,1} \times \frac{M_{CO_2}}{M_{CaO}} \quad (25)$$

where $M_{paper,t}$ is paper and paperboard production, $r_{LM,t}$ is the LM generation rate, $U_{LM,t}$ is the recycling and utilization rate, and $\bar{\gamma}_{LM,1}$ is the one-year pile-average CaO conversion fraction. Its literature-reported average and range are used in the Monte Carlo analysis.

For CS, uptake attributed to the annual stockpiled material flow is calculated as:

$$C_{CS,t} = M_{lime,t} \times L_{2,t} \times b_{3,t} \times p_{lime/CS,t} \times r_{CS,t} \times (1 - U_{CS,t}) \times f_{CaO,CS} \times \bar{\gamma}_{CS,1} \times \frac{M_{CO_2}}{M_{CaO}} \quad (26)$$

where $L_{2,t}$ is the fraction of lime used in the chemical sector, $b_{3,t}$ is the share allocated to calcium-carbide production, $p_{lime/CS,t}$ converts lime input to calcium-carbide output, $r_{CS,t}$ is the CS generation rate, $U_{CS,t}$ is the recycling and utilization rate, and $\bar{\gamma}_{CS,1}$ is the one-year pile-average CaO conversion fraction. Its literature-reported average and range are used in the Monte Carlo analysis.

### 2.3 Data Sources and Processing

Based on the published 1930-2020 lime carbon uptake dataset established by (Bing et al., 2023), we recalibrated China's lime production data for 1930-1995, expanded the lime-related basic activity data to nine additional countries, including the United Kingdom, France, Germany, Italy, Japan, Australia, Brazil, Russia, and Canada, and updated the dataset to 2024.

For the lime-related basic activity data, USGS statistics were used as the primary data backbone where available, followed by national statistical yearbooks, industry association reports, regression-based estimates, conversion-coefficient estimates, and linear interpolation for short data gaps. Where multiple sources overlapped, we systematically compared statistical units, product definitions, accounting boundaries, and year-to-year changes to identify missing observations, source inconsistencies, and implausible data changes. We acknowledge that combining activity data from different sources increases the complexity of uncertainty, especially because statistical boundaries, reporting practices, and data quality may differ among sources and periods.

#### 2.3.1. Lime Production Data

Before continuous USGS coverage, country-specific historical sources and transparent proxy methods were used. Japanese limestone shipments to lime manufacture reported by Shimanishi (2004) were converted to lime output using 1.8 t limestone per tonne of lime and checked against overlapping industry statistics. Brazilian lime production for 1940–1964 was taken from the IBGE Physical Production Tables (Produção de cal; IBGE, 2026), while 1930–1939 values are explicitly identified as autoregressive estimates. French, Canadian, German, and former Soviet records were compiled from national statistical yearbooks, with Canadian publications cited by their historical publication years (Dominion Bureau of Statistics, various years). Australian lime production was converted from limestone allocated to lime manufacture using a limestone-to-lime conversion coefficient of 0.24 (ABS, 2026). For Italy, a mean

limestone-to-lime coefficient of 0.24 was derived from years reporting both inputs and outputs. For the United Kingdom, fixed 1949-based allocation ratios of 0.161 for limestone and dolomite and 0.049 for chalk, together with a lime-yield coefficient of 0.225, were used for years lacking direct observations (Ordnance Survey, 1957). Short gaps in Russian records were linearly interpolated; for 1959–1991, Russian output was estimated as 0.54 of reported Soviet lime production (Upravlenie S. U. T. statisticheskoe, 1961). All source classifications, equations, diagnostics, and uncertainty assumptions are documented in Supplementary Table SI-2, Data 1.

To illustrate the source harmonization procedure, China's 1930–1995 lime-production series was reconstructed by linking three consecutive source segments: a limestone-proxy reconstruction for 1930–1949, a sectoral activity-based reconstruction for 1950–1985, and directly reported or association-based statistics for 1986–1995.

For 1930–1949, continuous national lime-production statistics were unavailable for China, particularly for 1930–1948. We therefore reconstructed annual lime production using limestone production as the primary proxy. Limestone production for mainland China and Northeast China was obtained from Guan (2007), which reports annual limestone production for 1912–1949. Observed lime-production records for Northeast China from *Manshu Kojo Tokei Sokuho, Showa 15 (Kotoku 7)* were used to calibrate the conversion relationship between limestone and lime production, yielding a limestone-to-lime conversion coefficient of 0.21. The calibrated relationship was then applied separately to mainland China and Northeast China, and the two regional estimates were combined to derive national lime production for 1930–1949.

For 1950–1985, we adopted a sectoral reconstruction approach constrained by activity data and historical evidence. Based on the sectoral lime-use shares reported by Liu (2018), total lime demand was allocated to the construction, iron and steel, calcium carbide, and alumina sectors. Steel, calcium carbide, and alumina production were used as activity indicators for their respective sectors, and through-origin proportional regression models were developed to estimate missing sectoral lime consumption. Construction lime demand was reconstructed using completed building floor area from Cao et al. (2019) as the activity proxy and constrained by historical information on lime production and application structure reported by Liao (1995), based on statistics from the China Lime Association.

For 1986–1995, lime production data were obtained from Liao (1995), based on China Lime Association statistics, and the *China Building Materials Statistical Yearbook*. Before merging the three source segments into a continuous historical series, statistical boundaries were harmonized through overlapping-year comparisons, consistency checks against sectoral activity indicators, and calibration of conversion coefficients where necessary to ensure temporal continuity and comparability. The harmonized series was subsequently linked with later statistical records to produce a continuous national dataset. All fitted parameters, reconstructed results, model diagnostics, and uncertainty distributions are documented in Supplementary Table SI-2 Data1.

This example illustrates how historical datasets with different statistical boundaries, reporting practices, and data availability were harmonized into a temporally consistent activity dataset before subsequent emission estimation and uncertainty analysis. To reflect the additional uncertainty introduced by source integration, source-specific uncertainty ranges

were assigned to reported statistics, regression-derived estimates, conversion-derived values, and interpolated data, and propagated through the Monte Carlo analysis (Section 2.4).

**2.3.2 Industrial Product Output Data**

For the period from 1930 to 2020, data on crude steel, alumina, and paper and paperboard sectors for China, the United States, and the global total were adopted from the source-prioritized and internally cross-checked activity dataset constructed by Bing et al (2023). For 2021–2024, data on crude steel and alumina for China, the United States, additional countries, and the global total were sourced from the USGS, while data on paper and paperboard were obtained from the *FAO Yearbook of Forest Products*. Specific data sources were organized as follows:

Crude steel and pig iron: Data for additional 9 countries from 1959 to 2024 were retrieved from the *USGS Iron and Steel Slag Database* (USGS, 2026b), while historical data from 1930 to 1958 were sourced from the British Geological Survey (BGS, 2026). Detailed datasets are provided in Supplementary Table SI-2 Data 2 and Data3.

Alumina: Data for additional 9 countries covering 1959–2024 were obtained from the USGS Bauxite and Alumina Database (USGS, 2026c). Data for the 1930–1958 period were derived from the British Geological Survey (BGS, 2026) and the *Statistical Yearbook of France* (ASF, 2026). Detailed datasets are provided in Supplementary Table SI-2 Data 4.

Paper and paperboard: Data from 1946 to 2024 were sourced from the FAO Yearbook of Forest Products (FAO, 2026), and data from 1930 to 1945 were obtained from the United Nations Statistical Yearbook (UNSD, 2026). Detailed datasets are provided in Supplementary Table SI-2 Data 5.

To improve transparency and reproducibility across the country, sector, and material dimensions, we added a methodological framework summary table (Table 1). The table lists the main activity-data sources, model or harmonization approach, and qualitative uncertainty rating for each accounting module. The uncertainty rating is defined as follows: A, directly reported and temporally consistent data with low parameter uncertainty; B, direct statistics supplemented by literature parameters or limited harmonization; C, mixed direct and reconstructed data requiring regression, conversion factors, or boundary adjustment; and D, sparse historical or residual estimates with high integration uncertainty.

514 Table 1. Summary of activity-data sources, accounting models, and qualitative uncertainty ratings used in the lime process-emission and carbonation-sink
515 framework.

| Category | Scope | Main data/model approach | Qualitative uncertainty | Detailed source |
|---|---|---|---|---|
| Lime production activity data | China, 1930-1995 | Segmented reconstruction linking limestone-proxy estimates (1930-1949), sectoral activity-based reconstruction (1950-1985), and reported/association statistics (1986-1995). | C-D before 1985; B after 1986 | SI-2 Data1 |
| | Nine additional countries before continuous USGS coverage | Priority use of national statistical yearbooks and historical sources; limestone/dolomite conversion ratios or interpolation used only where direct records are incomplete. | B-C for reported series; C-D for converted/interpolated series | SI-2 Data1 |
| | All countries, 1959-2024 where available | USGS statistics harmonized with historical national records and checked for temporal continuity. | B | SI-2 Data1 |
| Process-emission accounting | All countries and ROW | Country lime production allocated by sector and combined with lime-use ratios, localized CaO contents, and process-emission factors. | B-C | SI-3 Data1-7 |
| Carbonation sink accounting | Construction materials (LSS, MOR) | Slab/pile carbonation models using material allocation, CaO content, thickness, conversion fraction, and carbonation-rate parameters. | B-C | SI-3 Data8-11 |
| | Chemical materials (PCC, CS, SUG, LM) | Output/use rates, utilization ratios, CaO contents, conversion fractions, and carbonation-rate parameters. | B-C | SI-3 Data8-13 |
| | Metallurgical materials (SS, BFS, RM) | Industrial output, slag/red mud generation rates, utilization ratios, lime-origin allocation, and time-varying carbonation parameters. | C-D | SI-3 Data8-14 |

| | | | | |
|---|---|---|---|---|
| Uncertainty analysis | All countries, sectors, and materials | Monte Carlo propagation of activity-data uncertainty, source-integration uncertainty, emission factors, CaO contents, material allocation ratios, conversion fractions, carbonation rates, and regression/interpolation uncertainty. | Reported as 95% uncertainty interval | SI-3 Data1-17 |

Note: Qualitative uncertainty levels indicate data reliability and reconstruction intensity: A, directly reported and temporally complete statistics; B, direct statistics supplemented by literature parameters or minor harmonization; C, mixed direct and reconstructed data requiring conversion, regression, or interpolation; D, sparse historical data with substantial reconstruction or source-integration uncertainty. Detailed numerical distributions, fitted parameters, diagnostics, and uncertainty ranges are provided in the Supplementary Information.

## 2.4 Uncertainty Assessment

We identified 18 groups of factors affecting the estimation of process $CO_2$ emissions from lime production and carbonation uptake by lime-based materials, comprising 1,894 input parameters with specified statistical distributions (Supplementary Table SI-3, Data 1–15). Given the substantial uncertainty in these parameters, we applied the Monte Carlo method recommended by the 2006 IPCC Guidelines for National Greenhouse Gas Inventories. The statistical distributions of these variables were incorporated into the accounting model, and 10,000 Monte Carlo iterations were performed. Final estimates are reported as the median of the simulated distributions. The 2.5th and 97.5th percentiles define the lower and upper bounds, respectively, of the 95% uncertainty interval (UI).

Uncertainty introduced by historical activity-data reconstruction and source harmonization was explicitly included in the Monte Carlo framework. Source-specific uncertainty ranges were assigned according to data reliability, record completeness, and reconstruction method. Directly reported statistics were assigned narrower ranges than reconstructed data. For regression-derived estimates, uncertainty was characterized using model fitting errors, calibration diagnostics, and goodness-of-fit information reported in Supplementary Table SI-2 Data1. For conversion-derived and interpolated estimates, uncertainty ranges were assigned based on the corresponding activity-data and conversion-parameter uncertainties in Supplementary Table SI-3. Rather than introducing an additional standalone "source-integration" parameter that would be difficult to constrain independently, we incorporated discrepancies among overlapping datasets, uncertainty associated with limestone-to-lime conversion, differences in statistical boundaries, and regression-based reconstruction uncertainty into the uncertainty ranges assigned to historical activity data. This treatment differentiates complete statistical records from reconstructed, converted, and interpolated values, and allows uncertainty levels to vary among countries and time periods according to source quality.

During each Monte Carlo iteration, these activity-data uncertainty terms were jointly sampled with emission factors, CaO contents, material-use shares, carbonation ratios, and other model parameters, and then propagated through the process-emission and carbonation-uptake accounting models to generate distributions of annual and cumulative emissions, uptake, and net emissions.

No explicit cross-country or cross-parameter correlation matrix was imposed in the baseline Monte Carlo implementation; therefore, sampled variables were treated as independent within their assigned distributions, except for deterministic accounting relationships applied after sampling. We acknowledge that positive correlations may exist among some parameters, for example among countries using similar statistical sources or among material parameters governed by common industrial technologies. Accordingly, the reported 95% UIs should be interpreted as conditional on this independence assumption and may be narrower than intervals obtained under a fully correlated error structure. This limitation is now explicitly stated, and the reported aggregate uncertainty is not interpreted as evidence that subdivision alone improves data quality.

Compared with our previous research, this study incorporates refinements in four key aspects. (1) Regional refinement to enhance the dataset's representativeness. We separated the

United Kingdom, France, Germany, Italy, Russia, Japan, Brazil, Australia, and Canada from the rest-of-the-world (ROW) category used in previous studies. This allowed us to establish, for the first time, a lime carbonation sink dataset covering 11 countries, which collectively accounted for an average of 78.9% of global lime production (see Supplementary Table SI-2, Data 1). (2) More detailed, country-specific parameterization. The parameters were updated for lime $CO_2$ uptake in the newly added countries. The parameters include the proportion of lime usage across various sectors, the CaO content of different lime materials, and the production and utilization rates of lime materials. These improve the accuracy of the accounting compared to the $CO_2$ uptake parameters used for the ROW region in our previous work (see Supplementary Table SI-3, Data 1–15). (3) Inclusion of BFS in the accounting system. BFS was incorporated to address the previous omission of its carbonation contribution from metallurgical slags (see Supplementary Table SI-2, Data 3). (4) Data-constrained temporal and regional parameterization of SS and BFS. Complete annual and country-specific data were unavailable for the SS and BFS generation coefficients and for the fractions directed to road-base applications or open-air stockpiles. We therefore used four non-overlapping accounting periods: 1930–1949, 1950–1972, 1973–1999, and 2000–2024. These periods represent broad stages in iron- and steelmaking technology and serve only as common accounting windows; they do not imply synchronous technological transitions across countries. Crude steel and pig-iron production were obtained from statistical data and were not determined by these assumptions. Country-specific slag generation coefficients and pathway-allocation fractions were used where available. Otherwise, separate values were assigned to developed and developing regions based on differences in industrialization, technology-adoption timing, and slag-management practices. The parameter values, assumptions, and supporting references are provided in Supplementary Table SI-3, Data 8–9.

## 3. Results and Discussion

### 3.1 Global Process $CO_2$ Emissions from Lime Production

Figure 3 presents global process $CO_2$ emissions from lime production. Between 1930 and 2024, annual process emissions from the global lime industry increased substantially, from 18.5 Mt $CO_2$ $yr^{-1}$ (95% CI: 18.0–18.9 Mt $CO_2$ $yr^{-1}$) in 1930 to 299.2 Mt $CO_2$ $yr^{-1}$ (95% CI: 288.4–310.2 Mt $CO_2$ $yr^{-1}$) in 2024. Cumulative emissions over this period reached 11.3 Gt $CO_2$ (95% CI: 10.7–11.9 Gt $CO_2$; Fig. 3a). This increase was driven by continued global urbanization and industrialization and the resulting demand for lime in construction, metallurgy, the chemical industry, and environmental applications (Wu et al., 2024). Global lime production increased by approximately 394.6 Mt, from 25.4 Mt in 1930 to 420.0 Mt in 2024, equivalent to a 16.5-fold increase (U.S. Geological Survey, 2026; Supplementary Table SI-2, Data 1).

Global lime process emissions broadly followed the trend in lime production because lime production is the principal activity variable in the emission-accounting model. However, emissions increased more slowly than production because the production-weighted emission factor decreased over time. In the model, this emission factor varies with the allocation of lime among downstream sectors and the corresponding CaO contents of lime products. Therefore, the divergence between the growth rates of production and process emissions reflects changes in the modeled composition and sectoral use of lime rather than improvements in production technology.

Construction was the largest cumulative source of lime-related process emissions during 1930–2024 (Fig. 3b). Annual construction-sector emissions increased from 3.6 Mt $CO_2$ $yr^{-1}$ (95% CI: 2.4–5.2 Mt $CO_2$ $yr^{-1}$) in 1930 to 130.9 Mt $CO_2$ $yr^{-1}$ (95% CI: 97.7–164.2 Mt $CO_2$ $yr^{-1}$) in 2024. Cumulative construction-sector emissions reached 3.9 Gt $CO_2$ (95% CI: 2.9–4.9 Gt $CO_2$), accounting for 34.5% of total cumulative process emissions. Metallurgy was the second-largest contributor, with annual emissions increasing from 6.6 Mt $CO_2$ $yr^{-1}$ (95% CI: 5.5–7.7 Mt $CO_2$ $yr^{-1}$) in 1930 to 96.2 Mt $CO_2$ $yr^{-1}$ (95% CI: 65.3–129.5 Mt $CO_2$ $yr^{-1}$) in 2024. Cumulative metallurgical emissions reached 3.8 Gt $CO_2$ (95% CI: 2.9–4.7 Gt $CO_2$), representing 33.5% of the global total. Chemical-sector emissions increased from 3.6 Mt $CO_2$ $yr^{-1}$ (95% CI: 2.6–4.7 Mt $CO_2$ $yr^{-1}$) in 1930 to 45.4 Mt $CO_2$ $yr^{-1}$ (95% CI: 34.2–58.0 Mt $CO_2$ $yr^{-1}$) in 2024. Cumulative emissions from this sector reached 2.0 Gt $CO_2$ (95% CI: 1.5–2.4 Gt $CO_2$), accounting for 17.2% of total cumulative emissions. Cumulative emissions from other sectors amounted to 1.7 Gt $CO_2$ (95% CI: 1.3–2.7 Gt $CO_2$), representing the remaining 14.7%.

Process-emission trajectories differed substantially among countries between 1930 and 2024. Developed countries peaked at different times, ranging from 1964 in Germany and the 1970s–1980s in France, Japan, and the United Kingdom to 1999–2011 in Canada, the United States, Italy, and Australia, after which emissions generally declined. In the United States, emissions rebounded during the early 21st century, peaked in 2006, and subsequently decreased. In contrast, China and Brazil exhibited pronounced long-term growth, while Russia experienced a sharp decline following the dissolution of the Soviet Union and a partial rebound after 2000.

China was the largest contributor to both global lime production and associated process emissions. Its annual emissions increased from 0.4 Mt $CO_2$ $yr^{-1}$ (95% CI: 0.2–0.7 Mt $CO_2$ $yr^{-1}$) in 1930 to 226.7 Mt $CO_2$ $yr^{-1}$ (95% CI: 216.1–237.6 Mt $CO_2$ $yr^{-1}$) in 2024, corresponding to a compound annual growth rate of 6.9%. China's cumulative emissions reached 5.5 Gt $CO_2$ (95% CI: 4.9–6.0 Gt $CO_2$), accounting for 48.3% of the global total (Fig. 3b). The United States was the largest cumulative emitter among developed countries, with emissions of 953.9 Mt $CO_2$ (95% CI: 910.5–997.4 Mt $CO_2$), representing 8.4% of the global total. Russia and Germany contributed 611.1 and 605.4 Mt $CO_2$, respectively, each accounting for 5.4% of global cumulative emissions. Japan (370.2 Mt $CO_2$), Brazil (258.2 Mt $CO_2$), Italy (220.9 Mt $CO_2$), and France (189.2 Mt $CO_2$) contributed 3.3%, 2.3%, 2.0%, and 1.7%, respectively. Contributions from the United Kingdom (129.4 Mt $CO_2$), Canada (115.2 Mt $CO_2$), and Australia (76.4 Mt $CO_2$) were smaller, accounting for 1.1%, 1.0%, and 0.7%, respectively. Cumulative emissions from the rest of the world amounted to 2.3 Gt $CO_2$ (95% CI: 2.2–2.4 Gt $CO_2$), representing 20.5% of the global total (Fig. 3b).

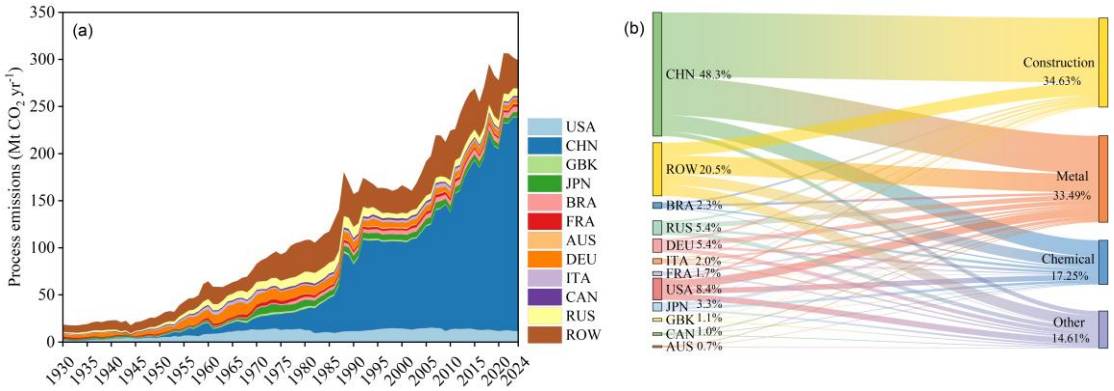


Fig. 3. Global process $CO_2$ emissions from lime production: (a) annual global emissions; and (b) cumulative emissions by country and sector.

### 3.2 Global Carbon Uptake by Lime Carbonation

The global lime carbonation sink increased from 4.1 Mt $CO_2$ $yr^{-1}$ (95% CI: 3.5–4.8 Mt $CO_2$ $yr^{-1}$) in 1930 to 136.1 Mt $CO_2$ $yr^{-1}$ (95% CI: 107.9–171.5 Mt $CO_2$ $yr^{-1}$) in 2024, corresponding to a compound annual growth rate of 3.8%. The cumulative carbonation sink over 1930–2024 reached 4.8 Gt $CO_2$ (95% CI: 3.9–5.8 Gt $CO_2$; Fig. 4a). Net emissions, calculated as process emissions minus carbonation uptake, increased from 14.3 Mt $CO_2$ $yr^{-1}$ in 1930 to 163.2 Mt $CO_2$ $yr^{-1}$ in 2024, resulting in cumulative net emissions of 6.5 Gt $CO_2$. Overall, lime-based materials reabsorbed approximately 42.2% of cumulative process emissions (Fig. 4b), 3.4 percentage points higher than the 38.8% estimate reported by Bing et al. (2023).

The 11 countries represented in this study contributed a cumulative carbonation sink of 3.7 Gt $CO_2$, accounting for 77.4% of the global total. Refinement of the activity data for nine additional countries reduced the share assigned to the aggregated rest-of-world region from 34.4% in Bing et al. (2023) to 22.6% in the present study (Fig. 4a). The accounting boundary was further refined by incorporating blast-furnace slag (BFS) and applying period-specific parameters to steel slag (SS) and BFS to reflect changes in iron- and steel-production practices.

The increasing carbon-offset level partly reflects the time lag between lime-material production and subsequent carbonation (Niu et al., 2024). Materials such as lime mortar (MOR), lime-stabilized soil (LSS), SS, and BFS do not attain their ultimate carbonation extent immediately and can continue to absorb $CO_2$ in subsequent years. Consequently, the annual carbonation sink includes both uptake by materials produced in the current year and continued uptake by materials inherited from previous years. In 2024, the lime carbonation sink was equivalent to approximately 1.5%–2.0% of the global terrestrial carbon sink in 2023 (Friedlingstein et al., 2025). Quantifying this anthropogenic carbonation sink provides data relevant to IPCC assessments and improves the completeness of the Global Carbon Budget.

Among the lime-derived materials considered, SS exhibited the largest cumulative carbon uptake, reaching 1.3 Gt $CO_2$ and accounting for 27.1% of the global cumulative carbonation sink (Fig. 4d). BFS and MOR followed, each contributing approximately 0.9 Gt $CO_2$ and accounting for 19.6% and 19.1%, respectively. Lime kiln dust (LKD) and LSS each contributed approximately 0.5 Gt $CO_2$, representing 9.8% and 9.6% of the global total, respectively. Together, these five materials contributed 4.1 Gt $CO_2$, accounting for 85.2% of the cumulative carbonation sink. Precipitated calcium carbonate (PCC), carbide slag (CS), and carbonation

sugar (SUG) contributed 0.3 Gt $CO_2$ (6.5%), 0.2 Gt $CO_2$ (4.5%), and 0.2 Gt $CO_2$ (3.8%), respectively. Contributions from red mud (RM) and lime mud (LM) were negligible, each accounting for less than 0.1% of the global total.

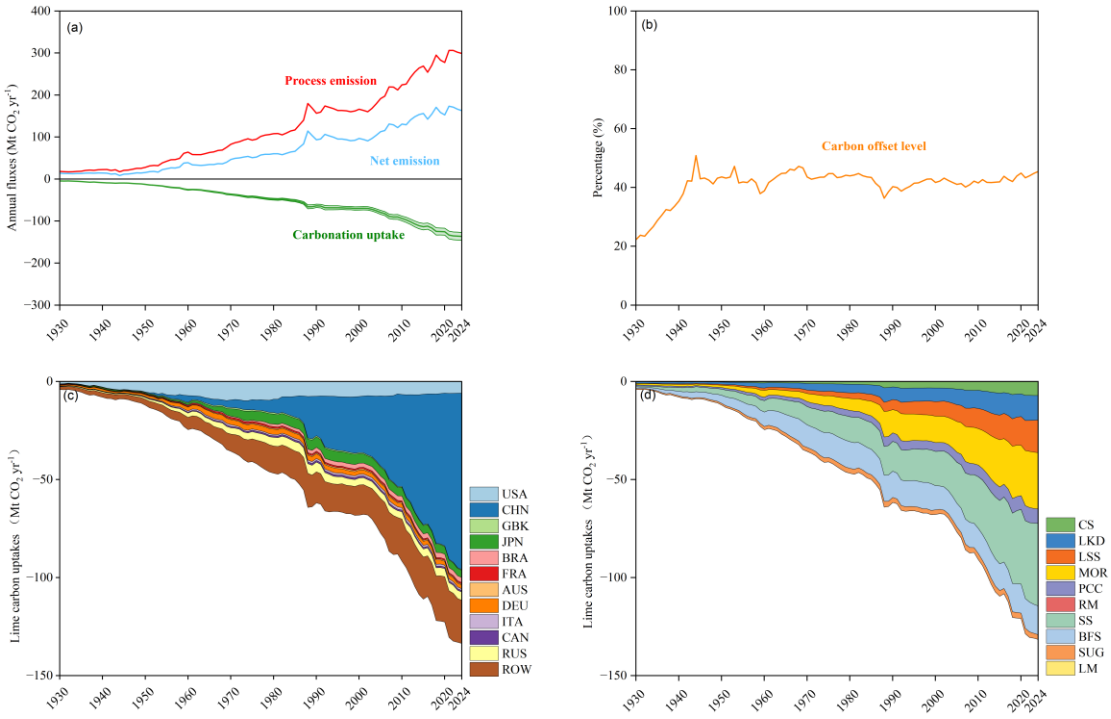


Fig. 4. Global lime carbon balance: (a) annual process emissions and carbonation uptake; (b) carbon-offset ratio (carbonation uptake divided by process emissions); (c) annual uptake by country and region; and (d) annual uptake by material.

China's annual lime carbonation sink increased markedly from 0.1 Mt $CO_2$ $yr^{-1}$ (95% CI: 0.04–0.2 Mt $CO_2$ $yr^{-1}$) in 1930 to 92.0 Mt $CO_2$ $yr^{-1}$ (95% CI: 65.8–125.6 Mt $CO_2$ $yr^{-1}$) in 2024. Its cumulative carbon uptake reached 1.9 Gt $CO_2$ (95% CI: 1.5–2.5 Gt $CO_2$), accounting for 40.7% of the global total (Fig. 4c). This dominant contribution was primarily associated with sustained lime demand from China's large-scale construction and iron and steel industries.

Among developed countries, the United States made the largest contribution. Its annual carbonation sink increased from 1.2 Mt $CO_2$ $yr^{-1}$ (95% CI: 0.8–1.7 Mt $CO_2$ $yr^{-1}$) in 1930 to 5.9 Mt $CO_2$ $yr^{-1}$ (95% CI: 4.4–7.7 Mt $CO_2$ $yr^{-1}$) in 2024. Its cumulative uptake reached 629.6 Mt $CO_2$ (95% CI: 456.2–843.5 Mt $CO_2$), equivalent to 13.2% of the global total.

Japan, Russia, Germany, Brazil, and Italy contributed cumulative carbonation sinks of 292.1, 271.7, 186.4, 113.6, and 67.4 Mt $CO_2$, respectively, corresponding to 6.1%, 5.7%, 3.9%, 2.4%, and 1.4% of the global total (Fig. 4c). France and Canada contributed 58.3 Mt $CO_2$ (1.2%) and 57.4 Mt $CO_2$ (1.2%), respectively. By contrast, the contributions from the United Kingdom and Australia were each below 1%, amounting to 40.5 Mt $CO_2$ (0.8%) and 33.9 Mt $CO_2$ (0.7%), respectively. The rest of the world collectively contributed 1.1 Gt $CO_2$, representing 22.6% of the global cumulative lime carbonation sink.

### 3.3 Global Lime Carbonation Sink in Different Industries

Industry-based analysis indicates that carbon uptake by lime-based materials generally increased across the major industrial sectors between 1930 and 2024. However, substantial

inter-sectoral differences were observed in the magnitude of the carbonation sink, dominant material types, and temporal trajectories (Fig. 5). The metallurgical sector was the largest contributor to the global lime carbonation sink, followed by construction and the chemical industry. Lime kiln dust (LKD), which is generated directly during lime production, was accounted for separately rather than allocated to a downstream industrial sector.

Carbon uptake in the metallurgical sector increased from 1.4 Mt $CO_2$ $yr^{-1}$ in 1930 (95% CI: 1.0–1.9 Mt $CO_2$ $yr^{-1}$) to 57.6 Mt $CO_2$ $yr^{-1}$ in 2024 (95% CI: 47.9–68.9 Mt $CO_2$ $yr^{-1}$). The cumulative carbonation sink over the study period reached 2.2 Gt $CO_2$ (95% CI: 1.9–2.6 Gt $CO_2$), accounting for 46.6% of the global lime carbonation sink (Fig. 5). Lime-derived materials generated during metallurgical processes, particularly steel slag (SS) and blast-furnace slag (BFS), provide a substantial material basis for mineral carbonation. With the sustained growth of global iron and steel production over the past century, the carbonation potential of metallurgical slags has increased considerably. By incorporating period-specific historical parameters, this study accounts for temporal and cross-country variations in the generation and utilization of metallurgical by-products, thereby improving the representation of the sector's historical carbonation sink. Previous studies have identified pronounced differences among countries in their management of steel slag and blast-furnace residues (Guo et al., 2018; Horii et al., 2015; O'Connor et al., 2021; USGS, 2026b). Developed countries generally established mature resource-utilization systems earlier, whereas developing countries have gradually shifted from long-term stockpiling toward more comprehensive utilization. Technological development and policy intervention have therefore played important roles in shaping the long-term evolution of the metallurgical carbonation sink.

The construction sector constituted the second-largest global lime carbonation sink. Annual carbon uptake increased from 0.8 Mt $CO_2$ $yr^{-1}$ in 1930 (95% CI: 0.5–1.2 Mt $CO_2$ $yr^{-1}$) to 48.4 Mt $CO_2$ $yr^{-1}$ in 2024 (95% CI: 25.4–80.2 Mt $CO_2$ $yr^{-1}$). The cumulative carbonation sink reached 1.4 Gt $CO_2$ (95% CI: 0.9–2.0 Gt $CO_2$), accounting for 28.8% of the global total (Fig. 5). This contribution primarily resulted from the widespread use of lime mortar (MOR) and lime-stabilized soil (LSS), together with their continued carbonation during service. Since the second half of the twentieth century, accelerating urbanization and infrastructure investment have substantially expanded the use of lime-based construction materials, driving a corresponding increase in carbon uptake (Manzoor and Yousuf, 2020).

The chemical industry made a smaller but relatively stable contribution. Its annual carbon uptake increased from 1.2 Mt $CO_2$ $yr^{-1}$ in 1930 (95% CI: 0.9–1.7 Mt $CO_2$ $yr^{-1}$) to 17.5 Mt $CO_2$ $yr^{-1}$ in 2024 (95% CI: 12.1–24.2 Mt $CO_2$ $yr^{-1}$). Cumulative uptake reached 0.7 Gt $CO_2$ (95% CI: 0.5–0.9 Gt $CO_2$), accounting for 14.8% of the global lime carbonation sink. Carbon uptake in this sector occurred mainly through industrial carbonation pathways involving carbide slag (CS), precipitated calcium carbonate (PCC), carbonation sugar (SUG), red mud (RM), and lime mud (LM).

LKD generated directly during lime production contributed the remaining 0.5 Gt $CO_2$, equivalent to 9.8% of the global cumulative carbonation sink. Because LKD is a production-stage by-product rather than a material associated with a specific downstream industry, it was reported separately from the metallurgical, construction, and chemical sectors.

From spatial perspective, industry-dominated patterns of lime carbon sequestration exhibit pronounced heterogeneity across countries and regions (Fig. 5). Developed countries (e.g., the United States, Japan, and major European nations), characterized by long histories of iron and steel production and well-established circular economy systems, have long been dominated by metallurgical-sector lime carbonation sink, with cumulative effects that are particularly evident on historical timescales (Spring and Cirella, 2022). In contrast, developing countries undergoing rapid industrialization and urbanization (e.g., China, Brazil, and parts of the rest-of-world regions) have experienced surging demand for lime-based materials in the construction sector, which has gradually become the primary regional source of lime-related carbon sequestration. In China, carbon uptake by lime materials in the construction sector accelerated markedly in the early twenty-first century, closely coinciding with the timing of rapid urbanization (Cai et al., 2020).

Overall, the differentiated global distribution of lime carbonation sink across industries and regions fundamentally reflects the combined influences of industrial structure, economic development pathways, resource utilization efficiency, and policy frameworks. Clarifying the relative contributions of different sectors and their underlying evolutionary mechanisms is of critical scientific importance for designing sector-specific carbon management strategies for enhancing the carbon sequestration potential of lime-based materials.

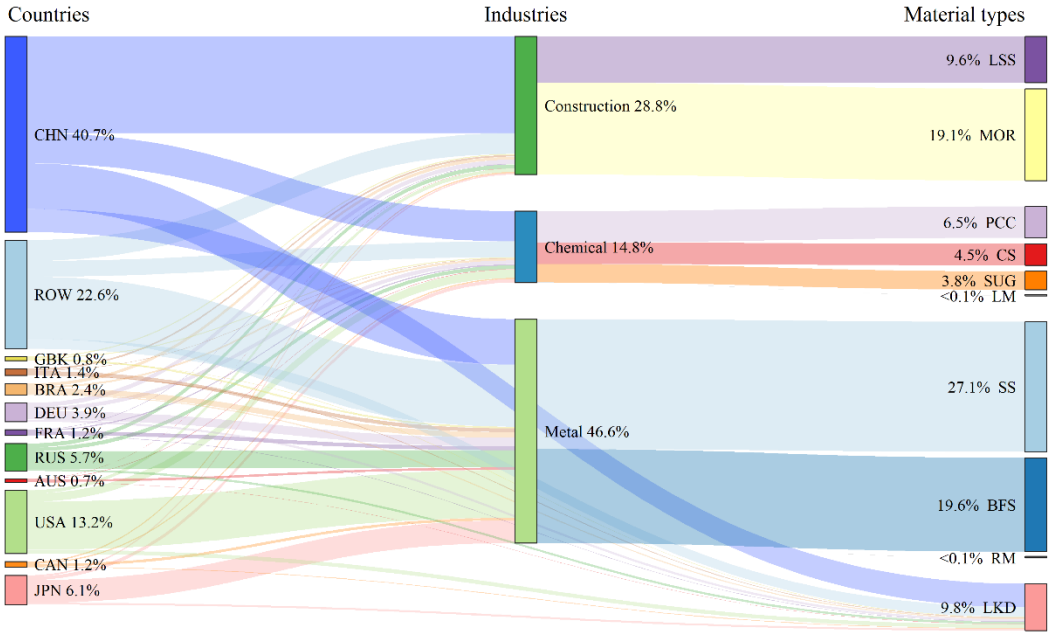


Fig. 5. Cumulative lime carbonation uptake by country, sector, and material, 1930–2024.

### 3.4 Time-Lag Effect of Lime Carbonation Sink

Both current-year and historical $CO_2$ uptake by global lime-based materials exhibited long-term increasing trends between 1930 and 2024, although interannual fluctuations occurred (Fig. 6a). “Current-year uptake” refers to $CO_2$ absorbed by materials produced in the corresponding year, whereas “historical uptake” represents continued $CO_2$ uptake in subsequent years by material cohorts produced in earlier years.

Mechanistically, the time-lag effect reflects the accumulation of legacy material stocks and

the progressive carbonation of reactive Ca-bearing phases. Within the accounting framework, annual uptake comprises uptake attributed to materials produced in the current year and continued uptake by incompletely carbonated materials inherited from previous years. For precipitated calcium carbonate (PCC) and carbonation sugar (SUG), carbonation is integral to the production process, and uptake is therefore assigned to the production year. Lime kiln dust (LKD), lime mud (LM), red mud (RM), and carbide slag (CS) are represented using literature-derived, one-year, pile-average CaO conversion parameters; this treatment does not assume complete conversion of CaO. By contrast, lime-stabilized soil (LSS) and lime mortar (MOR) follow the slab model, whereas steel slag (SS) and blast-furnace slag (BFS) follow the spherical-particle model and continue to carbonate over multiple years (Sect. 2.3.1–2.3.2).

As carbonation proceeds, the formation of a $CaCO_3$-rich product layer can impede inward $CO_2$ transport, shifting the reaction from relatively rapid initial uptake toward a slower, diffusion-controlled stage (Xi et al., 2016; Niu et al., 2025). For metallurgical slags, carbonation is further controlled by particle size, reactive Ca-bearing mineral phases, humidity, temperature, and stockpiling or reuse conditions (Zhao et al., 2025). Each year introduces a new cohort of lime-based materials, while incompletely carbonated cohorts from previous years continue to absorb $CO_2$. Over most of the study period, additions to this historical reactive stock exceeded its depletion, explaining the sustained increase in historical uptake. This mechanism also explains why carbonation sinks can decline more slowly than process emissions in countries that have already reached their emission peaks.

Current-year uptake increased from 4.1 Mt $CO_2$ $yr^{-1}$ in 1930 to 72.6 Mt $CO_2$ $yr^{-1}$ in 2024, corresponding to a compound annual growth rate of 3.1%. Cumulative current-year uptake reached 2.7 Gt $CO_2$, accounting for 56.2% of the total cumulative uptake. Historical uptake increased from 0.7 Mt $CO_2$ $yr^{-1}$ in 1931 to 63.5 Mt $CO_2$ $yr^{-1}$ in 2024, with a compound annual growth rate of 5.0%. Cumulative historical uptake reached 2.1 Gt $CO_2$, representing the remaining 43.8% (Fig. 6a).

MOR was the largest contributor to current-year uptake, accumulating 703.7 Mt $CO_2$ and accounting for 26.2% of cumulative current-year uptake, followed by LKD with 465.1 Mt $CO_2$ (17.3%). In contrast, SS dominated historical uptake, accumulating 949.3 Mt $CO_2$ and accounting for 45.3% of cumulative historical uptake, followed by BFS with 570.3 Mt $CO_2$ (27.2%) (Supplementary Table SI-1, Data 7–8). These results highlight the distinct temporal patterns of carbonation among lime-based materials (Fig. 6b). Historical uptake from SS and BFS exceeded their current-year uptake because these materials do not attain their material-specific maximum carbonation extent in the year they are generated, and substantial uptake therefore occurs gradually in subsequent years (Liu et al., 2018). Their natural carbonation rates are also influenced by environmental conditions, particularly temperature and humidity (Zhao et al., 2025). Future research could evaluate accelerated carbonation and $CO_2$ mineralization technologies within carbon capture, utilization, and storage frameworks to enhance controlled and verifiable $CO_2$ sequestration (Yang et al., 2022).

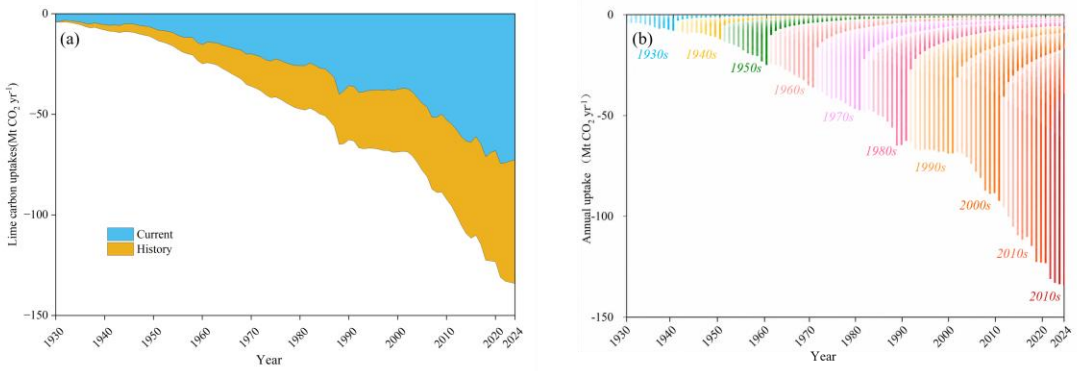


Fig. 6. Delayed effects of lime carbonation uptake, 1930–2024: (a) annual current-year and historical uptake; and (b) annual atmospheric $CO_2$ uptake disaggregated by production year.

### 3.5 Peaking Trajectories and Regional Disparities in Lime Carbon Balance

Based on lime process emissions and carbonation sink data, this study reveals significant regional heterogeneity in the global lime carbon balance: developed countries, represented by Europe, North America, Japan, and Australia, have generally achieved carbon peaking, whereas developing and transition economies show continued long-term growth or a post-2000 rebound in process emissions.

In developed countries, $CO_2$ emissions peaked between the 1960s and early 2010s. Germany (1964, 12.7 Mt $CO_2$), France (1974, 3.7 Mt $CO_2$), Japan (1973, 8.6 Mt $CO_2$), and the UK (1980, 2.9 Mt $CO_2$) peaked earlier, followed by Canada (1999, 1.9 Mt $CO_2$), the USA (2006, 15.6 Mt $CO_2$), Italy (2007, 4.4 Mt $CO_2$), and Australia (2011, 1.8 Mt $CO_2$). The carbon offset levels in their respective peak years were 21.6% for Germany, 25.6% for France, 57.0% for Japan, 24.1% for the UK, 50.6% for Canada, 48.1% for the USA, 30.0% for Italy, and 33.2% for Australia. Following the peak year, lime process emissions in these countries generally declined, with compound annual decline rates from the peak year to 2024 ranging from 0.8% to 5.2%. Carbonation sinks also tended to decrease with reductions in lime production, but the decline in carbon uptake was often less pronounced than that of process emissions because of the time-lag effect in the carbonation of certain lime-based materials. Consequently, carbon offset levels generally increased after the emission peak, helping to narrow net emissions from the lime production sector. This characteristic is closely related to mature secondary resource recycling systems and stringent climate policy constraints in developed countries (Dolphin et al., 2023), particularly the high recovery and comprehensive utilization of metallurgical by-products such as BFS and SS (Yi et al., 2012). In construction and civil engineering, substituting primary lime materials with these alkaline solid wastes can reduce process-related carbon emissions during production while maintaining carbonation sink potential through continuous mineral carbonation during their secondary-use phase (Pan et al., 2017).

Conversely, developing and transition economies exhibit continued growth pressure or emission rebound. China's lime process emissions increased from 0.4 Mt $CO_2$ $yr^{-1}$ in 1930 to 226.7 Mt $CO_2$ $yr^{-1}$ in 2024 (CAGR: 6.9%), with a post-2002 annual growth rate of 4.0%, driven by urbanization and infrastructure demand. China's carbonation sink reached 92.0 Mt $CO_2$ $yr^{-1}$ in 2024, corresponding to an offset level of 40.6%. Nevertheless, abatement pressure remains substantial because of the country's large absolute process emissions. Brazil's lime process

emissions also increased over the long term, reaching 5.9 Mt $CO_2$ $yr^{-1}$ in 2024, with an offset level of 44.3%, although emissions declined slightly from their 2013 peak of 6.1 Mt $CO_2$. Russia peaked during the Soviet era in 1988 at 12.2 Mt $CO_2$, but its emissions rebounded after 2000 (CAGR: 1.3%), reaching 8.0 Mt $CO_2$ $yr^{-1}$ in 2024, with an offset level of 52.8%. Lime process emission growth in these regions is mainly associated with infrastructure demand during industrialization and urbanization (Chen et al., 2022), while Russia's rebound is related to economic recovery and the restoration of industrial capacity after 2000.

In summary, regional differences in process emissions and carbonation sink trajectories reflect distinct development stages. Developed countries have achieved inflection points through industrial transformation, resource recycling, and policy intervention, whereas developing countries face the dual challenge of supporting economic growth while reducing process emissions. The divergence in carbon offset levels further reflects cross-country differences in the recycling efficiency and secondary utilization of lime-based materials.

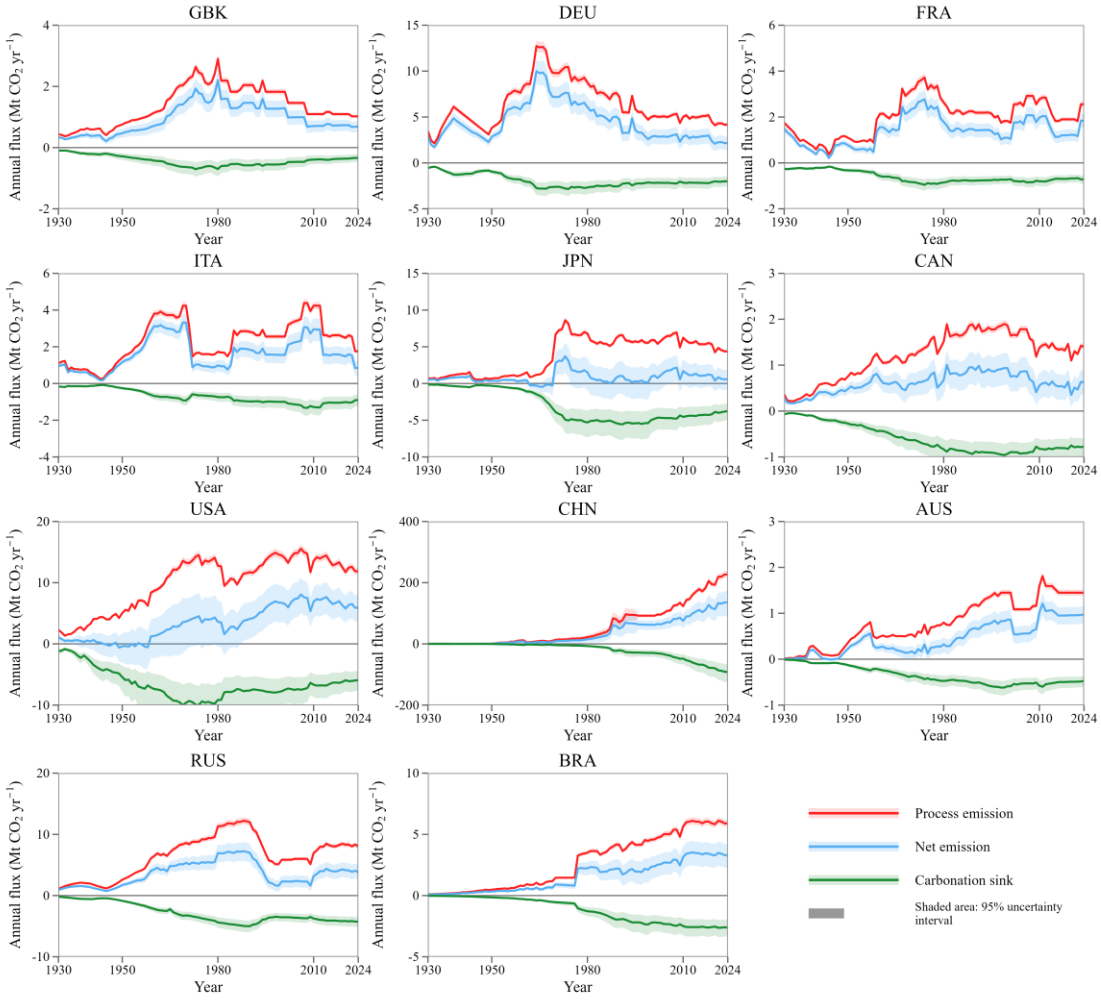


Fig. 7. Lime process emissions, carbonation uptake, and net emissions in 11 countries, 1930–2024.

### 3.6 Uncertainty Analysis

The uncertainty analysis in this study was designed to reflect data-source reliability, reconstruction intensity, and country-level heterogeneity. Building on the accounting model established by Xi et al. (2016) and the framework of Bing et al. (2023), probability distributions

were assigned to process-emission factors, CaO contents, material-use shares, carbonation ratios, activity data, and reconstruction parameters. In addition, source-specific uncertainty ranges were assigned to directly reported statistics, regression-derived estimates, conversion-derived estimates, and interpolated values. To show country-level differences in uncertainty, Fig. 6 presents the 95% uncertainty intervals for process emissions, carbonation sink, and net emissions across 11 countries. The corresponding uncertainty parameters are provided in Supplementary Table SI-3 Data1–15.

The results indicate that cumulative global lime process emissions from 1930 to 2024 were 11.3 Gt $CO_2$ (95% UI: 10.7–11.9 Gt $CO_2$), while the cumulative lime carbonation sink was 4.8 Gt $CO_2$ (95% UI: 3.9–5.8 Gt $CO_2$). The relative half-width of the 95% uncertainty interval was 5.1% for cumulative process emissions and 19.5% for cumulative carbonation sink, indicating that carbonation uptake is substantially more uncertain than process emissions. This larger uncertainty mainly arises from variability in CaO contents, carbonation rates, material-use allocation, utilization rates, time-lag parameters, and the additional uncertainty introduced during historical data-source harmonization.

Country-level uncertainty results further show that uncertainty is not uniform across regions or variables (Fig. 7). In 2024, the relative half-width of the 95% uncertainty intervals for process emissions across the 11 countries ranged from 4.5% to 4.8%, reflecting the dominant role of reported statistical data in recent emission estimates. In contrast, carbonation-sink uncertainty was larger, with relative half-widths ranging from 19.2% in Russia to 36.2% in the United Kingdom, because uptake estimates depend on material allocation, carbonation kinetics, and utilization assumptions. When emissions and uptake are similar in magnitude, net-emission uncertainty can be further amplified. These results indicate that the uncertainty framework used in this study captures important differences between original and reconstructed data, among countries, and between emission and uptake processes.

## 4. Data Availability

The datasets generated and analyzed in this study are available in the Zenodo repository: https://doi.org/10.57760/sciencedb.45314 (Bing et al., 2026). The dataset comprises three data files, including the results of lime-related carbon emissions and $CO_2$ uptake (Supplementary Table SI-1), basic activity data for lime-based materials (Supplementary Table SI-2), and uncertainty parameters associated with lime carbon emissions and $CO_2$ uptake (Supplementary Table SI-3).

## 5. Conclusion

In this study, we advanced the high-resolution accounting of global lime-related process emissions and carbonation uptake. For process-emission accounting, we extended the temporal coverage to 1930–2024 and refined the spatial resolution to 11 major lime-producing countries, collectively accounting for 78.9% of global lime production. By integrating country-specific activity data, sectoral lime-use structures, and localized CaO-content parameters, the framework provides a more detailed representation of process emissions across regions and downstream industries. Cumulative lime process emissions reached 11.3 Gt $CO_2$ (95% CI: 10.7–11.9 Gt $CO_2$) between 1930 and 2024. Construction was the largest source, contributing 3.9 Gt $CO_2$ (34.5%), followed by metallurgy with 3.8 Gt $CO_2$ (33.5%) and the chemical industry with 2.0 Gt $CO_2$ (17.2%). Process emissions continued to increase in developing regions,

indicating that reductions in absolute emissions remain necessary despite the partial offset provided by carbonation uptake.

For carbon uptake, the system boundary was refined by incorporating blast-furnace slag (BFS) into the lime-carbonation accounting framework and applying period-specific generation and utilization parameters to steel slag (SS) and BFS to represent historical changes in iron and steel production. Between 1930 and 2024, global lime-based materials cumulatively sequestered 4.8 Gt $CO_2$ (95% CI: 3.9–5.8 Gt $CO_2$), offsetting 42.2% of cumulative process emissions. The annual lime carbonation sink in 2024 was equivalent to approximately 1.5%–2.0% of the global terrestrial carbon sink in 2023. China was the largest contributor, with cumulative process emissions of 5.5 Gt $CO_2$ and cumulative carbonation uptake of 1.9 Gt $CO_2$, accounting for 48.3% and 40.7% of the corresponding global totals, respectively.

SS, BFS, lime mortar (MOR), lime kiln dust (LKD), and lime-stabilized soil (LSS) were the principal carbonation materials, contributing 27.1%, 19.6%, 19.1%, 9.8%, and 9.6% of the cumulative sink, respectively. Together, these five materials accounted for 85.2% of global cumulative carbonation uptake. SS and BFS were also the dominant contributors to historical uptake, accounting for 45.3% and 27.2%, respectively. This dominance arises because these materials do not attain their material-specific maximum carbonation extent in the year they are generated, and substantial $CO_2$ uptake therefore occurs gradually in subsequent years. These results provide an improved empirical basis for integrating lime-related process emissions and carbonation uptake into global carbon-budget assessments and for developing region- and material-specific mitigation strategies.

Regional divergence in lime carbonation uptake and net emissions is pronounced. In developing countries such as China and Brazil, carbonation uptake is mainly associated with construction-related materials and metallurgical by-products, while in developed regions such as the United States, metallurgical materials such as SS and BFS contribute substantially to the carbonation sink. Developed economies, including countries in Europe, the United States, Japan, and Australia, have generally passed their lime process-emission peaks, with declining gross emissions and net emissions gradually narrowing. In contrast, developing countries continue to show simultaneous growth in both emissions and uptake, and face increasing pressure from rising absolute emission volumes. These findings highlight the carbon-sink value of lime-based materials and provide an improved empirical basis for incorporating lime carbonation uptake into global carbon budget assessments and carbon-neutrality pathway analyses.

Future work should extend this historical dataset to scenario projections for 2025–2050 to better support global and national carbon-neutrality assessments. Such projections should consider changes in lime demand, regional industrial structure, kiln technology, material recycling rates, slag utilization, CCUS deployment, and enhanced-carbonation pathways. In particular, linking the lime carbonation sink dataset with national mitigation scenarios would help quantify the potential contribution of lime-based carbon uptake to net-zero roadmaps and identify priority countries, sectors, and material streams for future emission reduction and carbon sink enhancement (Simoni et al., 2022; EuLA, 2026a; NLA, 2026).

**Author Contributions.** F.X. designed and supervised the project. X.Z., with assistance from L.N., carried out data collection, organization, analysis, and database construction. L.B.

developed the accounting model and the associated computational codes. The manuscript was primarily drafted by X.Z. and L.B., and further improved through important suggestions and contributions from J.W., J.L., J.X., and Z.C.

**Competing interests**. The contact author has declared that none of the authors has any competing interests.

**Acknowledgements**. We thank our colleagues at the Institute of Applied Ecology, Chinese Academy of Sciences for their insightful discussions and technical support during the data collection and analysis phases. We extend special thanks to reviewer Robbie Andrew for his invaluable comments. We also deeply appreciate the constructive comments from the editors of *Earth System Science Data*, the anonymous reviewers, and the reviewers who provided feedback via the open online commentary, all of which have substantially improved the quality of this manuscript.

**Financial support**. This research was supported by Technology Innovation and Management of the Whole Process Green Development of Mineral Resources (No. 2023-JB-09-07), Joint Foundation Project of Liaoning Province, 2023-MSBA-141, the Major Program of the Institute for Applied Ecology of the Chinese Academy of Sciences (No. IAEMP202201), and Key Research and Development Project of Liaoning Province (No. 2025JH2/101330021).

**Reference**

Andrew, R. M.: Global $CO_2$ emissions from cement production, 1928–2018, Earth Syst. Sci. Data, 11, 1675–1710, https://doi.org/10.5194/essd-11-1675-2019, 2019.

Annuaire Statistique de la France (ASF): Annuaire Statistique de la France archives, available at: https://onlinebooks.library.upenn.edu/webbin/serial?id=annstatfr (last access: 18 January 2026), 2026.

Australian Bureau of Statistics (ABS): Year Book Australia archive, available at: https://www.abs.gov.au/ (last access: 18 January 2026), 2026.

Bing, L., Zhang, X., Wang, J., Niu, L., and Xi, F.: Global and National CO2 Emission from Lime Production Process and Carbonation sink from 1930 to 2024 (2.0), Zenodo [Data set], https://doi.org/10.5281/zenodo.18616060, 2026.

Brazilian Institute of Geography and Statistics (IBGE): Physical Production Tables, Economic Activities, Produção de cal, https://seculoxx.ibge.gov.br/economicas/atividades-economicas/tabelas-de-producao-fisica.html (last access: 18 January 2026), 2026.

British Geological Survey (BGS): World Mineral Statistics archive, available at: https://www.bgs.ac.uk/mineralsuk/statistics/world-mineral-statistics/world-mineral-statistics-archive/ (last access: 18 January 2026), 2026.

Bing, L., Ma, M., Liu, L., Wang, J., Niu, L., and Xi, F.: An investigation of the global uptake of $CO_2$ by lime from 1930 to 2020, Earth Syst. Sci. Data, 15, 2431–2444, https://doi.org/10.5194/essd-15-2431-2023 , 2023.

Cai, Z., Liu, Q., and Cao, S.: Real estate supports rapid development of China's urbanization, Land Use Policy, 95, 104582, https://doi.org/10.1016/j.landusepol.2020.104582 , 2020.
Cao, Z., Liu, G., Duan, H., Xi, F., Liu, G., and Yang, W.: Unravelling the mystery of Chinese building lifetime: A calibration and verification based on dynamic material flow analysis, Appl. Energy, 238, 442–452, https://doi.org/10.1016/j.apenergy.2019.01.106, 2019.
Campo, F. P., Tua, C., Biganzoli, L., Pantini, S., and Grosso, M.: Natural and enhanced carbonation of lime in its different applications: a review, Environ. Technol. Rev., 10, 224–237, https://doi.org/10.1080/21622515.2021.1982023, 2021.
Chen, C., Xu, R., Tong, D., Qin, X., Cheng, J., Liu, J., and Zhang, Q.: A striking growth of CO2 emissions from the global cement industry driven by new facilities in emerging countries, Environ. Res. Lett., 17, 044007, https://doi.org/10.1088/1748-9326/ac48b5, 2022.
Chukwuma, J. S., Pullin, H., and Renforth, P.: Assessing the carbon capture capacity of South Wales' legacy iron and steel slag, Miner. Eng., 173, 107232, https://doi.org/10.1016/j.mineng.2021.107232, 2021.
Crippa, M., Guizzardi, D., Pagani, F., Schiavina, M., Melchiorri, M., Pisoni, E., Graziosi, F., Muntean, M., Maes, J., Dijkstra, L., Van Damme, M., Clarisse, L., and Coheur, P.: Insights into the spatial distribution of global, national, and subnational greenhouse gas emissions in EDGAR v8.0, Earth Syst. Sci. Data, 16, 2811–2830, https://doi.org/10.5194/essd-16-2811-2024, 2024.
Davis, S. J., Lewis, N. S., Shaner, M., Aggarwal, S., Arent, D., Azevedo, I. L., Benson, S. M., Bradley, T., Brouwer, J., Chiang, Y.-M., Clack, C. T. M., Cohen, A., Doig, S., Edmonds, J., Fennell, P., Field, C. B., Hannegan, B., Hodge, B.-M., Hoffert, M. I., Ingersoll, E., Jaramillo, P., Lackner, K. S., Mach, K. J., Mastrandrea, M., Ogden, J., Peterson, P. F., Sanchez, D. L., Sperling, D., Stagner, J., Trancik, J. E., Yang, C.-J., and Caldeira, K.: Net-zero emissions energy systems, Science, 360, eaas9793, https://doi.org/10.1126/science.aas9793 , 2018.
Dolphin, G., Pahle, M., Burtraw, D., and Kosch, M.: A net-zero target compels a backward induction approach to climate policy, Nat. Clim. Change, 13, 1033–1041, https://doi.org/10.1038/s41558-023-01798-y, 2023.
Dominion Bureau of Statistics, Mining, Metallurgical and Chemical Branch: Historical statistical publications on lime production, Dominion Bureau of Statistics, Ottawa, Canada, various years, available at: https://publications.gc.ca/site/eng/9.847247/publication.html (last access: 18 January 2026).
Ellis, L. D., Badel, A. F., Chiang, M. L., Park, R. J.-Y., and Chiang, Y.-M.: Toward electrochemical synthesis of cement—An electrolyzer-based process for decarbonating $CaCO_3$ while producing useful gas streams, Proc. Natl. Acad. Sci., 117, 12584–12591, https://doi.org/10.1073/pnas.1821673116 , 2020.
Elyasi Gomari, K., Rezaei Gomari, S., Hughes, D., and Ahmed, T.: Exploring the potential of steel slag waste for carbon sequestration through mineral carbonation: a comparative study of blast-furnace slag and ladle slag, J. Environ. Manage., 351, 119835, https://doi.org/10.1016/j.jenvman.2023.119835, 2024.
European Lime Association (EuLA): A pathway to negative $CO_2$ emissions by 2050, available at: https://eula.eu/wp-content/uploads/2023/09/WEB_EULA-2030-Climate-Roadmap_Lime-

Acts_A4_v19.pdf (last access: 18 January 2026), 2026a.
European Commission. Joint Research Centre. Institute for Prospective Technological Studies.: Best available techniques (BAT) reference document for the production of cement, lime and magnesium oxide: Industrial Emissions Directive 2010/75/EU (integrated pollution prevention and control), Publications Office, LU, 2013.
Food and Agriculture Organization of the United Nations (FAO): Forestry production and trade statistics, available at: https://www.fao.org/forestry-fao/statistics/80570/en/ (last access: 18 January 2026), 2026.
Friedlingstein, P., O'Sullivan, M., Jones, M. W., Andrew, R. M., Gregor, L., Hauck, J., Le Quéré, C., Luijkx, I. T., Olsen, A., Peters, G. P., Peters, W., Pongratz, J., Schwingshackl, C., Sitch, S., Canadell, J. G., Ciais, P., Jackson, R. B., Alin, S. R., Alkama, R., Arneth, A., Arora, V. K., Bates, N. R., Becker, M., Bellouin, N., Bittig, H. C., Bopp, L., Chevallier, F., Chini, L. P., Cronin, M., Evans, W., Falk, S., Feely, R. A., Gasser, T., Gehlen, M., Gkritzalis, T., Gloege, L., Grassi, G., Gruber, N., Gürses, Ö., Harris, I., Hefner, M., Houghton, R. A., Hurtt, G. C., Iida, Y., Ilyina, T., Jain, A. K., Jersild, A., Kadono, K., Kato, E., Kennedy, D., Klein Goldewijk, K., Knauer, J., Korsbakken, J. I., Landschützer, P., Lefèvre, N., Lindsay, K., Liu, J., Liu, Z., Marland, G., Mayot, N., McGrath, M. J., Metzl, N., Monacci, N. M., Munro, D. R., Nakaoka, S.-I., Niwa, Y., O'Brien, K., Ono, T., Palmer, P. I., Pan, N., Pierrot, D., Pocock, K., Poulter, B., Resplandy, L., Robertson, E., Rödenbeck, C., Rodriguez, C., Rosan, T. M., Schwinger, J., Séférian, R., Shutler, J. D., Skjelvan, I., Steinhoff, T., Sun, Q., Sutton, A. J., Sweeney, C., Takao, S., Tanhua, T., Tans, P. P., Tian, X., Tian, H., Tilbrook, B., Tsujino, H., Tubiello, F., van der Werf, G. R., Walker, A. P., Wanninkhof, R., Whitehead, C., Willstrand Wranne, A., et al.: Global Carbon Budget 2022, Earth Syst. Sci. Data, 14, 4811–4900, https://doi.org/10.5194/essd-14-4811-2022 , 2022.
Friedlingstein, P., O'Sullivan, M., Jones, M. W., Andrew, R. M., Hauck, J., Landschützer, P., Le Quéré, C., Li, H., Luijkx, I. T., and Olsen, A.: Global Carbon Budget 2024, Earth Syst. Sci. Data, 17, 965–1039, https://doi.org/10.5194/essd-17-965-2025 , 2025.
Gilfillan, D. and Marland, G.: CDIAC-FF: Global and national $CO_2$ emissions from fossil fuel combustion and cement manufacture, 1751–2017, Earth Syst. Sci. Data, 13, 1667–1680, https://doi.org/10.5194/essd-13-1667-2021, 2021.
Gao, W., Zhou, W., Lyu, X., Liu, X., Su, H., Li, C., and Wang, H.: Comprehensive utilization of steel slag: A review, Powder Technol., 422, 118449, 2023.
Guan, Q. and Makino, F.: Estimates of Chinese mining output: 1912–1949, Discussion Paper D99-7, Institute of Economic Research, Hitotsubashi University, Kunitachi, Japan, 27 pp., 1999.
Guo, J., Bao, Y., and Wang, M.: Steel slag in China: Treatment, recycling, and management, Waste Manag., 78, 318–330, 2018.
Han, R., Wang, Y., Xing, S., Pang, C., Hao, Y., Song, C., and Liu, Q.: Progress in reducing calcination reaction temperature of Calcium-Looping CO2 capture technology: A critical review, Chem. Eng. J., 450, 137952, https://doi.org/10.1016/j.cej.2022.137952, 2022.
Hanein, T., Simoni, M., Woo, C. L., Provis, J. L., and Kinoshita, H.: Decarbonisation of calcium carbonate at atmospheric temperatures and pressures, with simultaneous $CO_2$ capture, through production of sodium carbonate, Energy Environ. Sci., 14, 6595–6604, 2021.
Heraiz, H., Li, J., Pan, Z., Zhang, D., Hu, Y., Mu, X., Baras, A., Liu, J., Ni, W., and Hitch, M.: The utilization of slag, steel slag, and desulfurization gypsum as binder systems in UHPC

with iron tailings and steel fibers: A review, Minerals, 15, 538, https://doi.org/10.3390/min15050538, 2025.
Horii, K., Tsutsumi, N., Kato, T., Kitano, Y., and Sugahara, K.: Overview of iron/steel slag application and development of new utilization technologies, Nippon Steel Sumitomo Met. Tech. Rep., 109, 5–11, 2015.
IPCC: IPCC guidelines for national greenhouse gas inventories, Institute for Global Environmental Strategies (IGES), Hayama (Japan), 2006.
Johannesson, B. and Utgenannt, P.: Microstructural changes caused by carbonation of cement mortar, *Cem. Concr. Res.*, 31, 925–931, 2001.
Laveglia, A., Ukrainczyk, N., De Belie, N., and Koenders, E.: Cradle-to-grave environmental and economic sustainability of lime-based plasters manufactured with upcycled materials, J. Clean. Prod., 452, 142088, https://doi.org/10.1016/j.jclepro.2024.142088, 2024a.
Liao, Y. and Yin, B.: Current status and future development goals of China's lime industry, New Build. Mater., 8, 2–5, 1995 (in Chinese).
Liu, L. L., Wang, J. Y., Bing, L. F., Ling, J. H., Xu, M., and Xi, F. M.: Analysis of carbon sink of steel slag in China., Ying Yong Sheng Tai Xue Bao J. Appl. Ecol., 29, 3385–3390, 2018.
Liu, Z., Guan, D., Wei, W., Davis, S. J., Ciais, P., Bai, J., Peng, S., Zhang, Q., Hubacek, K., and Marland, G.: Reduced carbon emission estimates from fossil fuel combustion and cement production in China, Nature, 524, 335–338, 2015.
Li, L., Ling, T.-C., and Pan, S.-Y.: Environmental benefit assessment of steel slag utilization and carbonation: a systematic review, Sci. Total Environ., 806, 150280, https://doi.org/10.1016/j.scitotenv.2021.150280 , 2022.
Ministry of Industry and Information Technology (MIIT): Implementation plan for achieving the carbon peak in the building materials industry, available at: https://www.gov.cn/zhengce/zhengceku/2022-11/08/content_5725353.htm (last access: 18 January 2026), 2026.
Manocha, S. and Ponchon, F.: Management of lime in steel, Metals, 8, 686, 2018.
Manzoor, S. O. and Yousuf, A.: Stabilisation of soils with lime: A review, J. Mater. Environ. Sci., 11, 1538–1551, 2020.
Muriithi, G. N., Petrik, L. F., Fatoba, O., Gitari, W. M., Doucet, F. J., Nel, J., Nyale, S. M., and Chuks, P. E.: Comparison of $CO_2$ capture by ex situ accelerated carbonation and in situ naturally weathered coal fly ash, J. Environ. Manage., 127, 212–220, https://doi.org/10.1016/j.jenvman.2013.05.027, 2013.
Naito, M., Takeda, K., and Matsui, Y.: Ironmaking technology for the last 100 years: deployment to advanced technologies from introduction of technological know-how, and evolution to next-generation process, ISIJ Int., 55, 7–35, 2015.
National Lime Association (NLA): A Roadmap to Carbon Neutrality for the U.S. Lime Industry, https://www.lime.org/wp-content/uploads/nla_lime_roadmap_final_01_july_24_cc.pdf (last access: 18 January 2026), 2026.
Ordnance Survey: Limestone, Planning Maps: Explanatory Texts No. 4, Ordnance Survey, Chessington, Surrey, UK, 1957, available at: https://maps.nls.uk/os/ten-mile/info.html (last access: 18 January 2026).
O'Connor, J., Nguyen, T. B. T., Honeyands, T., Monaghan, B., O'Dea, D., Rinklebe, J., Vinu,

A., Hoang, S. A., Singh, G., and Kirkham, M. B.: Production, characterisation, utilisation, and beneficial soil application of steel slag: A review, J. Hazard. Mater., 419, 126478, 2021.
Pan, S.-Y., Chung, T.-C., Ho, C.-C., Hou, C.-J., Chen, Y.-H., and Chiang, P.-C.: CO2 mineralization and utilization using steel slag for establishing a waste-to-resource supply chain, Sci. Rep., 7, 17227, 2017.
Pullin, H., Bray, A. W., Burke, I. T., Muir, D. D., Sapsford, D. J., Mayes, W. M., and Renforth, P.: Atmospheric carbon capture performance of legacy iron and steel waste, Environ. Sci. Technol., 53, 9502–9511, https://doi.org/10.1021/acs.est.9b01265, 2019.
Papadakis, V. G., Vayenas, C. G., and Fardis, M. N.: Experimental investigation and mathematical modeling of the concrete carbonation problem, Chem. Eng. Sci., 46, 1333–1338, 1991.
Ren, S., Aldahri, T., Liu, W., and Liang, B.: CO2 mineral sequestration by using blast furnace slag: From batch to continuous experiments, Energy, 214, 118975, 2021.
Revuelta, M. B.: Construction Materials: Geology, Production and Applications, Springer Nature, 602 pp., 2021.
Shimanishi, T.: A history of the limestone mining industry in the postwar period, based on LIMESTONE, a trade journal published by the Limestone Association of Japan, Mita Bus. Rev., 47, 115–138, 2004.
Simoni, M., Wilkes, M. D., Brown, S., Provis, J. L., Kinoshita, H., and Hanein, T.: Decarbonising the lime industry: State-of-the-art, Renew. Sustain. Energy Rev., 168, 112765, https://doi.org/10.1016/j.rser.2022.112765, 2022.
Spring, C. R. and Cirella, G. T.: Fostering Sustainable Development: Green Energy Policy in the European Union and the United States, in: Human Settlements, edited by: Cirella, G. T., Springer Singapore, Singapore, 101–137, https://doi.org/10.1007/978-981-16-4031-5_7, 2022.
United States Geological Survey (USGS): Lime Statistics and Information | U.S. Geological Survey: https://www.usgs.gov/centers/national-minerals-information-center/lime-statistics-and-information, last access: 18 January 2026a.
United States Geological Survey (USGS): Iron and Steel Slag Statistics and Information | U.S. Geological Survey: https://www.usgs.gov/centers/national-minerals-information-center/iron-and-steel-slag-statistics-and-information, last access: 18 January 2026b.
United States Geological Survey (USGS): Bauxite and Alumina Statistics and Information | U.S. Geological Survey: https://www.usgs.gov/centers/national-minerals-information-center/bauxite-and-alumina-statistics-and-information, last access: 18 January 2026c.
United Nations Statistics Division (UNSD): Statistical Yearbook, available at: https://unstats.un.org/UNSDWebsite/Publications/StatisticalYearbook/ (last access: 18 January 2026), 2026.
United Nations Human Settlements Programme (UN-Habitat): World Cities Report 2022: Envisaging the Future of Cities, Nairobi, UN-Habitat, 2022, 422 pp., available at: https://unhabitat.org/wcr/2022 , last access: 18 January 2026.
Upravlenie S. U. T. statisticheskoe: National economy of the USSR: statistical yearbook, U.S. Joint Publications Research Service, Washington, DC, USA, 866 pp., 1961.
Wang, Q.-L. and Shen, F.-E.: Progress and application of calcium carbonate produced by the

precipitation method, Mater. Sci. Eng. (Hangzhou), 20, 306–312, 2002.
Wu, S., Shao, Z., Andrew, R. M., Bing, L., Wang, J., Niu, L., Liu, Z., and Xi, F.: Global CO2 uptake by cement materials accounts 1930–2023, Sci. Data, 11, 1409, 2024.
Xi, F., Davis, S. J., Ciais, P., Crawford-Brown, D., Guan, D., Pade, C., Shi, T., Syddall, M., Lv, J., and Ji, L.: Substantial global carbon uptake by cement carbonation, Nat. Geosci., 9, 880–883, 2016.
Xu, R., Tong, D., Xiao, Q., Qin, X., Chen, C., Yan, L., Cheng, J., Cui, C., Hu, H., Liu, W., Yan, X., Wang, H., Liu, X., Geng, G., Lei, Y., Guan, D., He, K., and Zhang, Q.: MEIC-global-$CO_2$: A new global $CO_2$ emission inventory with highly resolved source-category and sub-country information, Sci. China Earth Sci., 67, 450–465, https://doi.org/10.1007/s11430-023-1230-3, 2024.
Xi, F., Ma, M., Davis, S. J., Bing, L., Wang, J., Niu, L., Liu, G., Shao, A., Gu, W., and Liu, Z.: Natural carbonation of alkaline industrial wastes: A large-scale, unaccounted sink for $CO_2$, Research Square [preprint], https://doi.org/10.21203/rs.3.rs-5763182/v1, 2025.
Yang, Y., Holappa, L., Saxen, H., and van der Stel, J.: Ironmaking, in: Treatise on process metallurgy, Elsevier, 7–88, 2024.
Yi, H., Xu, G., Cheng, H., Wang, J., Wan, Y., and Chen, H.: An overview of utilization of steel slag, Procedia Environ. Sci., 16, 791–801, 2012.
Zhao, Q., Liu, C., Mei, X., Saxén, H., and Zevenhoven, R.: Research progress of steel slag-based carbon sequestration, Fundam. Res., 5, 282–287, 2025.